

Online Inference for Mixture Model of Streaming Graph Signals with Non-White Excitation

Yiran He, Hoi-To Wai

Abstract—This paper considers a joint multi-graph inference and clustering problem for simultaneous inference of node centrality and association of graph signals with their graphs. We study a mixture model of filtered low pass graph signals with possibly non-white and low-rank excitation. While the mixture model is motivated from practical scenarios, it presents significant challenges to prior graph learning methods. As a remedy, we consider an inference problem focusing on the node centrality of graphs. We design an expectation-maximization (EM) algorithm with a unique low-rank plus sparse prior derived from low pass signal property. We propose a novel online EM algorithm for inference from streaming data. As an example, we extend the online algorithm to detect if the signals are generated from an abnormal graph. We show that the proposed algorithms converge to a stationary point of the maximum-a-posterior (MAP) problem. Numerical experiments support our analysis.

Index Terms—blind centrality inference, clustering of graph signals, expectation maximization, online graph learning

I. INTRODUCTION

The increasing demands for extracting information from complex systems have motivated the study of graphical models in many disciplines such as social science, biology, and data science. To analyze graph signals, i.e., observations made on the *nodes*, graph signal processing (GSP) [2], [3] has emerged as a natural framework for signal processing applications such as denoising [4], sampling [5], etc. Importantly, studies on graph topology learning using graph signal observations have been reported. Popular methods are proposed based on smoothness [6], [7], spectral template [8], topological constraints [9], causal modeling [10], nonlinear model [11], [12], partial observations [13]; see the overview papers [14], [15]. Moreover, a recent direction is to perform end-to-end learning for features of graph topology. The subjects of interest include centrality [16], [17], communities [18], [19], network processes [20], [21], etc. Compared to traditional graph learning, the latter approaches are robust to challenging but realistic scenarios such as when the excitation is not white noise, or when the graph signals are not sufficiently smooth.

Many existing results on graph learning focus on a setting where the goal is to infer a single graph from data. In reality, the data can be more complex and is related to multiple graphs. For example, recent works [22]–[27] studied the time varying graph learning problem when the topology changes slowly.

A preliminary version of this work has been presented at ICASSP 2022, Marina Bay Sands, Singapore [1]. Y. He and H.-T. Wai are with the Department of SEEM, The Chinese University of Hong Kong, Shatin, Hong Kong SAR of China. E-mails: yrhe@se.cuhk.edu.hk, htwai@se.cuhk.edu.hk. This work is supported in part by RGC Project #24203520.

Alternatively, one also considers the scenario where the graph topology differ significantly across samples. For example, a series of resting state brain networks have been identified from brain signals [28]; stock prices recorded at different states of the market may lead to different graph topology [29]. This model is also relevant to the problem of detecting topology changes in graph signals [30]–[33].

This paper treats a *joint multi-graph centrality inference and clustering* problem which simultaneously infers the node centrality of multiple graphs and clusters observed signals with respect to the graph that generates them. Our problem is motivated by applications involving multiple graphs with unknown associations between the graphs and observations. For example, when observing brain signals, we do not know which state the subject is in; for stock prices observations, the states of the market can be difficult to identify. While centrality inference can be performed by prior works [16], [17], the clustering problem is more challenging as classical algorithms such as spectral clustering [34], KNN [35] do not consider structures in the graph signal observations which is crucial to providing a reliable estimates. Recent works have developed algorithms that focus on simultaneous clustering and graph topology learning, e.g., graph Laplacian mixture model [36] and its regularized version [37], regularized spectral clustering [38], K -means based method [39]. Most of these works are developed from the Gaussian Markov random field model and entail stringent conditions such as requiring the observations to be generated from full-rank, white excitation. In comparison, our approach handles a relaxed mixture model of graph signal with possibly low-rank, non-white excitation.

The current paper also proposes an *online algorithm* for the joint inference problem from streaming data. Notice that many existing graph learning algorithms require batch data. This is in contrast to the practical environment that involves streaming and even dynamical data collection. Furthermore, the online algorithm enjoys a low memory footprint and computation complexity by processing data on-the-fly. Several online algorithms on graph topology learning have been proposed, e.g., for time varying graph learning [40]–[42], for multi-graph topology learning but with pre-clustered data [43]. In contrast, our algorithm is the first to perform multi-graph inference and clustering simultaneously and in an online fashion. Our key contributions are:

- To study graph signals observations based on multiple graphs, we propose a mixture model of graph signals with general non-white excitation. Moreover, the model supports missing data and general observation model such as the logit

model for inference from binary data.

- We formulate a joint inference and clustering problem via the MAP framework to infer node centrality and cluster observations according to the graphs. We design a batch EM algorithm under a unique low-rank plus sparse prior. We show that the EM algorithm converges to a stationary point at a sublinear rate. The algorithm supports efficient implementation for inference in the mixture model.
- We develop a novel online EM algorithm based on the stochastic approximation (SA) scheme for streaming data. The algorithm processes each of the incoming observation on-the-fly and features a low memory footprint while delivering similar performances as the batch EM. Our analysis shows that any fixed point of the algorithm is a stationary point of MAP. We also describe an application of the online algorithm to blind anomaly detection.
- We perform numerical experiments on synthetic and real data from brain and stock markets. The efficacy of the proposed algorithms support our findings.

Compared to the conference version [1], this paper considers an extended signal model with missing data and logit observations. We also propose an online algorithm for streaming data and provide an extended set of experiments.

Organization. This paper is organized as follows. In Sec. II, we describe the mixture model of graph signals and then formally introduce the joint inference problem. Furthermore, we develop a maximum-a-posterior formulation with low-rank plus sparse prior that adapts to the low pass signal property. In Sec. III, we propose a batch EM algorithm for Gaussian and logit observations. In Sec. IV, we introduce an online EM algorithm for streaming data and discuss its application to online anomaly detection. Finally, numerical experiments are presented to support our findings in Sec. V.

Notations. We use boldfaced character (resp. boldfaced capital letter) to denote vector (resp. matrix). For any vector $\mathbf{x} \in \mathbb{R}^n$, $\|\mathbf{x}\|$, $\|\mathbf{x}\|_1$ denote the Euclidean, ℓ_1 norm, respectively. For any matrix $\mathbf{X} \in \mathbb{R}^{m \times n}$, we take $[\mathbf{X}]_{i,j}$ to denote its (i, j) th entry. $\|\mathbf{X}\|$, $\|\mathbf{X}\|_1$, $\|\mathbf{X}\|_*$ denote the spectral norm, 1-norm, nuclear norm, respectively.

II. PROBLEM STATEMENT

Consider C undirected graphs $G^{(c)} = (\mathcal{V}, \mathcal{E}^{(c)}, \mathbf{A}^{(c)})$, $c = 1, \dots, C$. They share the same node set $\mathcal{V} := \{1, \dots, n\}$ but with different edge sets $\{\mathcal{E}^{(c)}\}_{c=1}^C \subseteq \mathcal{V} \times \mathcal{V}$. Each graph $G^{(c)}$ is endowed with a symmetric weighted adjacency matrix $\mathbf{A}^{(c)} \in \mathbb{R}_+^{n \times n}$ where $A_{ij}^{(c)} > 0$ if and only if $(i, j) \in \mathcal{E}^{(c)}$; otherwise, $A_{ij}^{(c)} = 0$. Define the eigenvalue decomposition (EVD) $\mathbf{A}^{(c)} = \mathbf{V}^{(c)} \mathbf{\Lambda}^{(c)} [\mathbf{V}^{(c)}]^\top$ where $\mathbf{V}^{(c)}$ is an orthogonal matrix and $\mathbf{\Lambda}^{(c)} = \text{Diag}(\boldsymbol{\lambda}^{(c)})$ contains its eigenvalues in descending order as: $\lambda_1^{(c)} \geq \dots \geq \lambda_n^{(c)}$. In this paper, we consider graphs that differ from each other in terms of their sets of central nodes. We adopt the notion of eigen-centrality to measure the latter. For graph $G^{(c)}$, its centrality vector is given by the top eigenvector $\mathbf{v}_1^{(c)}$. Node i is said to be more *central* if the magnitude of its centrality value is greater.

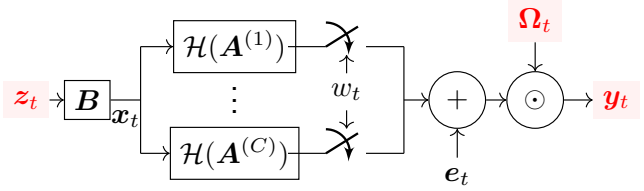


Fig. 1: Generation process for the mixture model of graph signals (2). Black (resp. red) color denotes unknown (resp. known) variables [cf. Problem 1].

We observe the graph signals on \mathcal{V} generated from a process defined on one of the graphs. These graph processes are described via the linear graph filters [2]: for $c = 1, \dots, C$,

$$\mathcal{H}(\mathbf{A}^{(c)}) = \sum_{\tau=0}^{P-1} h_\tau [\mathbf{A}^{(c)}]^\tau \in \mathbb{R}^{n \times n}, \quad (1)$$

where $\{h_\tau\}_{\tau=0}^{P-1}$ are the filter coefficients, $P \in \mathbb{Z}_+ \cup \{\infty\}$ is the filter's order. Each observation is indexed by $t \in \mathbb{Z}_+$ and is modeled as a graph signal matched with an identifier variable $w_t \in \{1, \dots, C\}$. The latter indicates that the graph signal is generated from $G^{(w_t)}$. We describe the observation via a *mixture model of graph signals* with missing data:

$$\mathbf{y}_t = \boldsymbol{\Omega}_t \odot \left\{ \sum_{c=1}^C \mathbb{1}(w_t = c) \mathcal{H}(\mathbf{A}^{(c)}) \mathbf{x}_t + \mathbf{e}_t \right\}. \quad (2a)$$

$$\mathbf{x}_t = \mathbf{B} \mathbf{z}_t = \sum_{j=1}^r \mathbf{b}_j [\mathbf{z}_t]_j. \quad (2b)$$

In (2a), $\mathbf{x}_t \in \mathbb{R}^n$ is the excitation to the graph filter to be described later, $\mathbf{e}_t \sim \mathcal{N}(\mathbf{0}, \sigma^2 \mathbf{I})$ is a Gaussian observation noise, $\mathbb{1}(\cdot)$ is the $\{0, 1\}$ indicator function, and \odot is the element-wise product. The vector $\mathcal{H}(\mathbf{A}^{(c)}) \mathbf{x}_t$ is the output of the graph filter $\mathcal{H}(\mathbf{A}^{(c)})$ with the excitation \mathbf{x}_t . The graph identifier w_t is a multinomial random variable (r.v.) with probability mass function $\mathbb{P}(w_t = c) = P_c$. The binary vector $\boldsymbol{\Omega}_t \in \{0, 1\}^n$ models on which nodes the signal values are missing in the current sample. An extension to logit observations will be described in Sec. III-A.

In (2b), we further model that the excitation signal \mathbf{x}_t lies in a general r -dimensional subspace $\text{span}\{\mathbf{B}\}$ with $\mathbf{B} \in \mathbb{R}^{n \times r}$, $r \leq n$. The setting is in line with real world observations as data tends to be low-rank [44]. The vector $\mathbf{z}_t \in \mathbb{R}^r$ is an excitation parameter whose element represents an observable source of stimuli on the graph process. Each column \mathbf{b}_j is the influence profile from the j th source $\mathbf{z}_{t,j}$ on the node set \mathcal{V} . For instance, \mathbf{B} can be modeled as a sparse matrix in this regard. Fig. 1 summarizes the generation process¹ of (2).

The fact that \mathbf{B} can be non-identity has made it challenging, if not impossible, to perform inference on (2) such as reconstructing the graph topology $\mathbf{A}^{(c)}$ from the filtered graph signals. Note that even in the single graph setting, prior methods [6]–[9] require the graph filter to be excited by white noise, i.e., with $\mathbf{B} = \mathbf{I}$. As a remedy inspired by [16]–[19], we aim to perform partial inference on (2) via the *joint multi-graph centrality inference and clustering* problem:

¹We remark that it is easy to extend (2) to the setting that every graph filter has different filter coefficients, every graph is associated with a different excitation subspace matrix $\mathbf{B}^{(c)}$, etc.

Problem 1 Given the data tuples $\{\text{DP}_t\}_t := \{\mathbf{y}_t, \mathbf{z}_t, \mathbf{\Omega}_t\}_t$ from (2), estimate (A) eigen-centrality vector $\mathbf{v}_1^{(c)}$ for each graph, and (B) identifier variable $w_t \in \{1, \dots, C\}$ for each sample (subject to permutation ambiguity).

We consider two settings of data availability. In the first setting, the data tuples are available in a *complete batch*, i.e., one observes $\{\text{DP}_t\}_{t=1}^m$ where m denotes the total number of samples. In the second setting, the data tuples are revealed in a *streaming fashion*. At time t , we only observe a sample DP_t that is generated randomly according to (2). To avoid degeneracy, we assume that different graphs are equipped with different sets of central nodes such that $\mathbf{v}_1^{(c)} \neq \mathbf{v}_1^{(c')}$, $c \neq c'$. We concentrate on graphs with small groups of central nodes of high-intra and low-inter connectivity. Such graphs typically admit a core-periphery structure which can be characterized by the eigengap condition $\lambda_1^{(c)} \gg \lambda_2^{(c)}$ [45].

Tackling the joint inference problem is challenging due to the large number of unknowns in the model (2). For instance, even with $C = 1$, inferring the eigen-centrality vector $\mathbf{v}_1^{(1)}$ from (2) is difficult since the graph filter $\mathcal{H}(\mathbf{A}^{(1)})$, the excitation subspace \mathbf{B} , etc., are unknown.

Remark 1 The requirement for excitation parameters $\{\mathbf{z}_t\}_t$ to be known may appear restrictive. However, we note in several applications, estimate of these parameters can be obtained as side information. For example, stock networks are excited by the market's interest level on various topics which can be estimated by the popularity of keywords on Google Trend. The excitation can also be endogenous such that $\{\mathbf{z}_t\}_t$ is approximated by observations on a subset of nodes. See Sec. V-C for two example applications using real data.

A. MAP Estimation with Reparametrization

This sub-section proposes a reparameterization technique to leverage the signal structure for finding a robust solution to Problem 1. We then formulate the maximum-a-priori (MAP) problem which will be the focus for the rest of this paper.

In the absence of knowledge on graph filters, Problem 1 will be ill-defined due to difficulty in extracting $\mathbf{v}_1^{(c)}$. Taking inspirations from [16], [17], we consider a low pass assumption [2], [46] on the underlying graph filters:

Assumption 1 The graph filter $\mathcal{H}(\mathbf{A}^{(c)})$, is 1-low pass with:

$$\eta^{(c)} := \max_{j=2, \dots, n} |h(\lambda_j^{(c)})| / |h(\lambda_1^{(c)})| < 1, \quad (3)$$

for $c = 1, \dots, C$, where the polynomial $h(\lambda) := \sum_{\tau=0}^{P-1} h_\tau \lambda^\tau$ is the frequency response of the graph filter $\mathcal{H}(\cdot)$.

The low pass ratio $\eta^{(c)}$ characterizes the strength of $\mathcal{H}(\mathbf{A}^{(c)})$. With a smaller $\eta^{(c)}$, the filter $\mathcal{H}(\mathbf{A}^{(c)})$ attenuates the signal components beyond the *cutoff frequency* $\lambda_1^{(c)}$ more. If $\eta^{(c)} \approx 1$, then $\mathcal{H}(\mathbf{A}^{(c)})$ is considered as *weak low pass*; if $\eta^{(c)} \ll 1$, then $\mathcal{H}(\mathbf{A}^{(c)})$ is considered as *strong low pass*. Assumption 1 is common in modeling network processes. Examples include, but are not limited to, opinion dynamics in social networks, stock dynamics, power systems, etc., see [46].

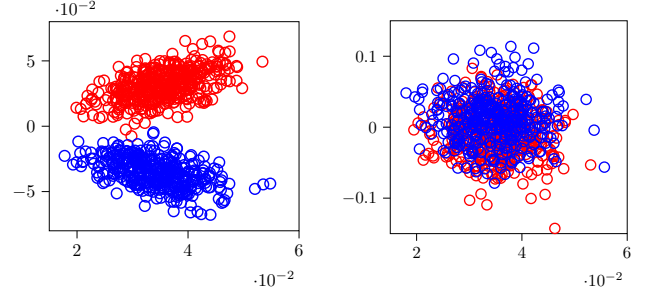


Fig. 2: Toy Example illustrating the data from two core periphery graphs. (Left) Strong low pass filter $\mathcal{H}_s(\mathbf{A}) = (\mathbf{I} - \frac{1}{40}\mathbf{A})^{-1}$; (Right) Weak low pass filter $\mathcal{H}_w(\mathbf{A}) = (\mathbf{I} - \frac{1}{80}\mathbf{A})^{-1}$.

Assumption 1 implies that the top eigenvector of $\mathcal{H}(\mathbf{A}^{(c)})$ corresponds to the centrality vector $\mathbf{v}_1^{(c)}$. Together with the condition that $\mathbf{v}_1^{(c)} \neq \mathbf{v}_1^{(c')}$, one may tackle Problem 1 through separating the $m (\gg C)$ observations into C clusters using naïve spectral clustering. Particularly, assume that $\mathbf{\Omega}_t = \mathbf{1}$, the (t, t') th element of the correlation matrix of observations is

$$\langle \mathbf{y}_t | \mathbf{y}_{t'} \rangle \approx \langle \mathcal{H}(\mathbf{A}^{(w_t)}) \mathbf{B} \mathbf{z}_t | \mathcal{H}(\mathbf{A}^{(w_{t'})}) \mathbf{B} \mathbf{z}_{t'} \rangle \quad (4)$$

Since the top eigenvectors of $\mathcal{H}(\mathbf{A}^{(w_t)})$, $\mathcal{H}(\mathbf{A}^{(w_{t'})})$ differ only if $w_t \neq w_{t'}$, the $m \times m$ correlation matrix shall exhibit a block structure aligned with the graph identifiers $\{w_t\}_{t=1}^m$.

To this end, an intuitive idea is to apply spectral clustering (SC) on the correlation matrix $\widehat{\mathbf{C}}_Y = [\mathbf{y}_1, \dots, \mathbf{y}_m]^\top [\mathbf{y}_1, \dots, \mathbf{y}_m]$ to cluster the graph signals. However, as demonstrated below, the result is sensitive to the low pass filter modeling the graph process:

Example 1 We generate $C = 2$ core-periphery graphs with $n = 100$ nodes, each with 10 distinct central nodes that are fully connected, and $m = 400C$ graph signals are generated according to (2). Fig. 2 shows the scatter plot whose coordinates of the $m = 400C$ points are taken to be the top/second eigen-vectors of $\widehat{\mathbf{C}}_Y$ and colored according to the true graph identifiers $\{w_t\}_{t=1}^m$. For the stronger low pass filter [Fig. 2 (left)], the data points are found to be clearly clustered. For the weaker low pass filter [Fig. 2 (right)], the data points cannot be clustered. In the latter case, applying naïve SC would result in erroneously clustered observations.

The naïve spectral clustering essentially utilizes difference in the subspaces $\text{span}\{\mathcal{H}(\mathbf{A}^{(c)})\mathbf{B}\}$, $c = 1, \dots, C$ to discern samples from different graphs. While such strategy is successful when $\mathcal{H}(\mathbf{A}^{(c)})$ is strong low pass, it may not work when the filter is weak low pass; see Remark 2 for further justifications. Nevertheless, the above example shows that inferring the natural parameters $\{\mathcal{H}(\mathbf{A}^{(c)})\mathbf{B}\}_{c=1}^C$ can be insufficient for a robust solution to Problem 1.

Particularly, the above example demonstrates that it is necessary to jointly consider the signal structure while clustering the graph signals. Our idea is to model and extract the hidden component(s) in $\mathcal{H}(\mathbf{A}^{(c)})\mathbf{B}$ that are indicative of the eigen-centrality vector, which thus provides the graph identifiers necessary for clustering. Observe the decomposition:

$$\mathcal{H}(\mathbf{A}^{(c)})\mathbf{B} = (\mathcal{H}(\mathbf{A}^{(c)}) - \rho\mathbf{I})\mathbf{B} + \rho\mathbf{B} \equiv \mathbf{L}_c + \mathbf{B}_\rho, \quad (5)$$

for any $\rho \geq 0$. The component $\mathbf{L}_c = (\mathcal{H}(\mathbf{A}^{(c)}) - \rho \mathbf{I})\mathbf{B}$ depends on the shifted graph filter $\mathcal{H}(\mathbf{A}^{(c)}) - \rho \mathbf{I}$. It is shown [18, Observation 1] that there exists $\rho > 0$ where the shifted graph filter enjoys a strictly lower low pass ratio, denoted as $\tilde{\eta}^{(c)}$, than the original ratio $\eta^{(c)}$. For example, with $\mathcal{H}(\mathbf{A}^{(c)}) = (\mathbf{I} - \alpha \mathbf{A}^{(c)})^{-1}$, it can be shown that the shifted graph filter with $\rho = 1$ has the low pass ratio of $\tilde{\eta}^{(c)} \leq \frac{\lambda_2^{(c)}}{\lambda_1^{(c)}} \eta^{(c)} \ll \eta^{(c)}$, provided that $\lambda_1^{(c)} \gg \lambda_2^{(c)}$ which can be satisfied for graphs with core-periphery structure [45]. Consequently, the matrix \mathbf{L}_c will be approximately rank-one.

Below, we show that the low-rank components \mathbf{L}_c are distinct for the different graphs that they are associated with. Assume without loss of generality (w.l.o.g.) that $(\tilde{\mathbf{v}}_1^{(c)})^\top \mathbf{v}_1^{(c)} \geq 0$, the following lemma is adapted from [17, Corollary 1]:

Lemma 1 For each $c = 1, \dots, C$, if $(\mathbf{v}_1^{(c)})^\top \mathbf{B} \mathbf{q}_1^{(c)} \neq 0$, then

$$\|\tilde{\mathbf{v}}_1^{(c)} - \mathbf{v}_1^{(c)}\| \leq \sqrt{2} \tilde{\eta}^{(c)} \frac{\|(\mathbf{V}_{n-1}^{(c)})^\top \mathbf{B} \mathbf{q}_1^{(c)}\|}{|(\mathbf{v}_1^{(c)})^\top \mathbf{B} \mathbf{q}_1^{(c)}|}, \quad (6)$$

where $\mathbf{V}_{n-1}^{(c)}$ is the last $n-1$ eigenvectors of $\mathbf{A}^{(c)}$, and $\tilde{\mathbf{v}}_1^{(c)}, \mathbf{q}_1^{(c)}$ are the top left, right singular vector of \mathbf{L}_c .

The right hand side of (6) is bounded by $\mathcal{O}(\tilde{\eta}^{(c)})$ with $\tilde{\eta}^{(c)} \ll 1$. Together with the observation that \mathbf{L}_c is approximately rank one, we obtain $\mathbf{L}_c \propto \mathbf{v}_1^{(c)} (\mathbf{q}_1^{(c)})^\top$. With the condition $\mathbf{v}_1^{(c)} \neq \mathbf{v}_1^{(c')}$, we observe that \mathbf{L}_c provides an effective indicator to distinguish the samples with different graph identifiers.

Establishing that \mathbf{L}_c is low rank may not be sufficient for its recovery in (5), where extra structure has to be leveraged for the residual term $\rho \mathbf{B}$ as inspired by [47]. Fortunately, since \mathbf{B} models the influences from external sources on the graph(s), we note from the applications described in [17], [18] that \mathbf{B} admits certain low-dimensional structure. For example, \mathbf{B} can be sparse, the number of non-zero row/column vectors of \mathbf{B} can be small, etc. As such, herein we model \mathbf{B} to be a sparse matrix which includes the special case of $\mathbf{B} = \mathbf{I}$. We observe that the matrix product $\mathcal{H}(\mathbf{A}^{(c)})\mathbf{B}$ admits a ‘low-rank plus sparse’ structure under the said premises.

MAP Estimation. The above motivates us to explicitly account for the implicit components $\mathbf{L}_c, \mathbf{B}_\rho$ during the inference process through a careful re-parameterization. Denote $\Theta := \{\{\mathbf{L}_c\}_{c=1}^C, \mathbf{B}_\rho, \{P_c\}_{c=1}^C\}$ as the set of parameters. We yield the following *structured* MAP estimation problem:

$$\max_{\Theta \in \mathfrak{T}} \mathcal{L}(\Theta) := \mathbb{E}[\log p(\mathbf{Y}|\Theta, \mathbf{Z}, \mathbf{\Omega})] + \log p(\Theta), \quad (7)$$

where $\mathfrak{T} = \{\Theta : P_c \geq 0, \sum_{c=1}^C P_c = 1\}$ and $p(\Theta)$ models the prior on Θ with the ‘low-rank plus sparse’ structure of $\mathbf{L}_c, \mathbf{B}_\rho$. A natural choice for the prior distribution is

$$p(\Theta) \propto \exp(-\lambda_S \|\mathbf{B}_\rho\|_1 - \lambda_L \sum_{c=1}^C \|\mathbf{L}_c\|_*), \quad (8)$$

where $\lambda_S, \lambda_L \geq 0$ are regularization parameters. Furthermore, the expectation $\mathbb{E}[\cdot]$ is defined w.r.t. the observation law for $\mathbf{Y}, \mathbf{Z}, \mathbf{\Omega}$ and the log-likelihood function is given by:

$$\log p(\mathbf{y}|\Theta, \mathbf{z}, \mathbf{\Omega}) = \log \left(\sum_{c=1}^C P_c e^{-\frac{1}{2\sigma^2} \|\mathbf{y} - \mathbf{\Omega} \odot (\mathbf{L}_c + \mathbf{B}_\rho) \mathbf{z}\|^2} \right) + \text{constant}, \quad (9)$$

which is non-concave due to the nonlinear coupling between $P_c, \mathbf{L}_c, \mathbf{B}_\rho$, making direct optimization of (7) intractable.

We notice that EM algorithms for classical models such as Gaussian Mixture Model (GMM) cannot be directly applied to (7). The reason is that (7) entails regularization terms for the ‘low-rank plus sparse’ structure. Additionally, the missing data and excitation parameter \mathbf{z}_t have to be incorporated into the inference process. In the next section, we concentrate on developing effective algorithms for (7) via the EM paradigm.

Remark 2 The poor performance of naive SC with weak low pass filter can be explained by [17, Lemma 2]. Under mild conditions, the latter lemma shows:

$$\|\mathbf{L}_c\| / \|\mathbf{B}_\rho\| \lesssim (1 - \eta^{(c)}) / (1 + \eta^{(c)}), \quad (10)$$

where $\mathbf{L}_c, \mathbf{B}_\rho$ are defined in (5). Now, if $\eta^{(c)} \approx 1$, we have $\mathcal{H}(\mathbf{A}^{(c)})\mathbf{B} \approx \mathbf{B}_\rho$ for any $c = 1, \dots, C$. Consequently, the correlation matrix $\mathbf{Y}^\top \mathbf{Y}$ does not have the anticipated block structure that is necessary for successful clustering.

III. BATCH EM ALGORITHM

This section develops a customized EM algorithm that is efficient to implement and enjoys desirable theoretical convergence properties. Particularly, we focus on *batch* data where m samples $\{\text{DP}_t\}_{t=1}^m$ are available all at once.

To begin, let us fix $\tilde{\Theta} = \{\{\tilde{\mathbf{L}}_c\}_{c=1}^C, \tilde{\mathbf{B}}_\rho, \{\tilde{P}_c\}_{c=1}^C\}$ and denote the conditional probability mass function for the latent r.v. w_t as $q(\cdot|\tilde{\Theta}, \text{DP}_t)$. The Jensen’s inequality implies the following lower bound on the log-likelihood term in (7):

$$\begin{aligned} & \log p(\mathbf{y}_t|\Theta, \mathbf{z}_t, \mathbf{\Omega}_t) \\ &= \log \left(\sum_{c=1}^C p(\mathbf{y}_t, w_t = c|\Theta, \mathbf{z}_t, \mathbf{\Omega}_t) \frac{q(w_t = c|\tilde{\Theta}, \text{DP}_t)}{q(w_t = c|\tilde{\Theta}, \text{DP}_t)} \right) \\ &\geq \mathbb{E}_{w_t \sim q(\cdot|\tilde{\Theta}, \text{DP}_t)} [\log p(\mathbf{y}_t, w_t|\Theta, \mathbf{z}_t, \mathbf{\Omega}_t)] + \zeta(\tilde{\Theta}), \end{aligned} \quad (11)$$

where $\zeta(\tilde{\Theta})$ is a function that only depends on the fixed $\tilde{\Theta}$. Taking the batch data setting into consideration, the above led us to the batch surrogate optimization problem:

$$\begin{aligned} & \max_{\Theta} \frac{1}{m} \sum_{t=1}^m \mathbb{E}_{w_t \sim q(\cdot|\tilde{\Theta}, \text{DP}_t)} [\log p(\mathbf{y}_t, w_t|\Theta, \mathbf{z}_t, \mathbf{\Omega}_t)] \\ & \quad - \lambda_S \|\mathbf{B}_\rho\|_1 - \lambda_L \sum_{c=1}^C \|\mathbf{L}_c\|_* \\ & \text{s.t. } \sum_{c=1}^C P_c = 1, P_c \geq 0, c = 1, \dots, C. \end{aligned} \quad (12)$$

Let us take a closer look at the first term in the objective function of (12). For $t = 1, \dots, m$, the Bayes’ rule implies

$$\begin{aligned} & \mathbb{E}_{w_t \sim q(\cdot|\tilde{\Theta}, \text{DP}_t)} [\log p(\mathbf{y}_t, w_t|\Theta, \mathbf{z}_t, \mathbf{\Omega}_t)] \\ &= \mathbb{E}_{w_t} [\mathbb{1}(w_t = c) \log \mathbb{P}(w_t = c) p(\mathbf{y}_t|\Theta, \mathbf{z}_t, \mathbf{\Omega}_t, w_t = c)] \\ &= \mathbb{E}_{w_t} [\mathbb{1}(w_t = c) \{\log(P_c) + \log p(\mathbf{y}_t|\mathbf{B}_\rho, \mathbf{L}_c, \mathbf{z}_t, \mathbf{\Omega}_t)\}], \end{aligned}$$

where we used $\mathbb{P}(w_t = c) = P_c$ and the dependence on $q(\cdot|\tilde{\Theta}, \text{DP}_t)$ were omitted for brevity. Moreover,

$$\begin{aligned} & \log p(\mathbf{y}_t|\mathbf{B}_\rho, \mathbf{L}_c, \mathbf{z}_t, \mathbf{\Omega}_t) \\ &= \frac{\langle \mathbf{\Omega}_t \odot (\mathbf{L}_c + \mathbf{B}_\rho) \mathbf{z}_t | \mathbf{y}_t \rangle}{\sigma^2} - \frac{\|\mathbf{\Omega}_t \odot (\mathbf{L}_c + \mathbf{B}_\rho) \mathbf{z}_t\|^2}{2\sigma^2} + \tilde{\zeta}_t(\tilde{\Theta}). \end{aligned} \quad (13)$$

where $\tilde{\zeta}_t(\tilde{\Theta}) := \zeta(\tilde{\Theta}) + \frac{1}{2\sigma^2} \|\mathbf{y}_t\|^2$. The above expressions can be simplified as

$$\begin{aligned} \langle \mathbf{\Omega}_t \odot (\mathbf{L}_c + \mathbf{B}_\rho) \mathbf{z}_t | \mathbf{y}_t \rangle &= \text{Tr}((\mathbf{L}_c + \mathbf{B}_\rho)^\top \mathbf{\Omega}_t \odot \mathbf{y}_t \mathbf{z}_t^\top), \\ \|\mathbf{\Omega}_t \odot (\mathbf{L}_c + \mathbf{B}_\rho) \mathbf{z}_t\|^2 &= \sum_{i=1}^n \text{Tr}((\mathbf{L}_c + \mathbf{B}_\rho)^\top \mathbf{e}_i \mathbf{e}_i^\top (\mathbf{L}_c + \mathbf{B}_\rho) \mathbf{\Omega}_{t,i} \mathbf{z}_t \mathbf{z}_t^\top). \end{aligned}$$

Define the conditional probability for the event that the t th data tuple is associated to the c th graph:

$$\begin{aligned} p_c(\tilde{\Theta}, \text{DP}_t) &:= \mathbb{E}_{w_t \sim q(\cdot | \tilde{\Theta}, \text{DP}_t)} [\mathbb{1}(w_t = c)] \\ &= \frac{\tilde{P}_c \exp(\frac{-1}{2\sigma^2} \|(\mathbf{y}_t - \mathbf{\Omega}_t \odot (\tilde{\mathbf{B}}_\rho + \tilde{\mathbf{L}}_c) \mathbf{z}_t)\|^2)}{\sum_{c'=1}^C \tilde{P}_{c'} \exp(\frac{-1}{2\sigma^2} \|(\mathbf{y}_t - \mathbf{\Omega}_t \odot (\tilde{\mathbf{B}}_\rho + \tilde{\mathbf{L}}_{c'}) \mathbf{z}_t)\|^2)}. \end{aligned} \quad (14)$$

and the sufficient statistics:

$$\begin{aligned} \overline{P}_c^{\tilde{\Theta}} &= \frac{1}{m} \sum_{t=1}^m p_c(\tilde{\Theta}, \text{DP}_t), \\ \overline{\mathbf{Y}\mathbf{Z}}_c^{\tilde{\Theta}} &= \frac{1}{m} \sum_{t=1}^m p_c(\tilde{\Theta}, \text{DP}_t) \mathbf{\Omega}_t \odot \mathbf{y}_t \mathbf{z}_t^\top, \\ \overline{\mathbf{Z}\mathbf{Z}}_{c,i}^{\tilde{\Theta}} &= \frac{1}{m} \sum_{t=1}^m p_c(\tilde{\Theta}, \text{DP}_t) \mathbf{\Omega}_{t,i} \mathbf{z}_t \mathbf{z}_t^\top. \end{aligned} \quad (15)$$

For any $\tilde{\Theta} \in \mathfrak{T}$, the lower bound surrogate objective function of (12) can be written as

$$\begin{aligned} \tilde{\mathcal{L}}(\Theta | \tilde{\Theta}) &= \tilde{\zeta}(\tilde{\Theta}) - \lambda_S \|\mathbf{B}_\rho\|_1 - \sum_{c=1}^C \lambda_L \|\mathbf{L}_c\|_* \\ &+ \sum_{c=1}^C \left\{ \overline{P}_c^{\tilde{\Theta}} \log(P_c) + \frac{1}{\sigma^2} \text{Tr}((\mathbf{L}_c + \mathbf{B}_\rho)^\top \overline{\mathbf{Y}\mathbf{Z}}_c^{\tilde{\Theta}}) \right. \\ &\left. - \frac{1}{2\sigma^2} \sum_{i=1}^n \text{Tr}((\mathbf{L}_c + \mathbf{B}_\rho)^\top \mathbf{e}_i \mathbf{e}_i^\top (\mathbf{L}_c + \mathbf{B}_\rho) \overline{\mathbf{Z}\mathbf{Z}}_{c,i}^{\tilde{\Theta}}) \right\}, \end{aligned} \quad (16)$$

which is a concave function in Θ and we have defined $\tilde{\zeta}(\tilde{\Theta}) = (1/m) \sum_{t=1}^m \tilde{\zeta}_t(\tilde{\Theta})$. For any $\Theta, \tilde{\Theta} \in \mathfrak{T}$, notice that it holds

$$\mathcal{L}(\Theta) \geq \tilde{\mathcal{L}}(\Theta | \tilde{\Theta}), \quad \mathcal{L}(\Theta) = \tilde{\mathcal{L}}(\Theta | \Theta). \quad (17)$$

The above derivations led us to a regularized (batch) EM algorithm. In particular, we initialize by fixing Θ^0 and evaluate the sufficient statistics using (15). Then, we alternate between the M-step and the E-step — in the M-step, we optimize w.r.t. Θ for the surrogate problem (12); in the E-step, we update the sufficient statistics using (15) through the new Θ . The overall algorithm is summarized in Algorithm 1.

Denote $\text{D}(\Theta | \tilde{\Theta}) := \mathcal{L}(\Theta) - \tilde{\mathcal{L}}(\Theta | \tilde{\Theta}) \geq 0$ as the difference function between $\mathcal{L}(\Theta)$ and the surrogate. We observe:

Proposition 1 Consider the sequence $\{\Theta^k\}_{k \geq 0}$ generated by Algorithm 1. The following holds:

1) The regularized log-likelihood value is non-decreasing:

$$\mathcal{L}(\Theta^{k+1}) \geq \mathcal{L}(\Theta^k), \quad \forall k \geq 0. \quad (19)$$

2) If the gradient w.r.t. Θ for the difference function $\text{D}(\Theta | \tilde{\Theta})$ is L -Lipschitz continuous, then for any $K_{\max} \geq 1$,

$$\min_{k=1, \dots, K_{\max}} \|\nabla_{\Theta} \text{D}(\Theta^k | \Theta^{k-1})\|^2 = \mathcal{O}(L/K_{\max}). \quad (20)$$

In addition, the directional derivative:

$$\mathcal{L}'(\tilde{\Theta}; \Theta - \tilde{\Theta}) := \lim_{\delta \rightarrow 0} \frac{\mathcal{L}(\tilde{\Theta} + \delta(\Theta - \tilde{\Theta})) - \mathcal{L}(\tilde{\Theta})}{\delta} \quad (21)$$

Algorithm 1 Batch EM for Partial Inference on (2)

- 1: **Input:** graph signals \mathbf{Y} , excitation parameters \mathbf{Z} , missing-information vectors $\{\mathbf{\Omega}_t\}_{t=1}^m$, no. of graphs C .
 - 2: **if** $\Theta^0 := \{\{\mathbf{L}_c^0\}_{c=1}^C, \mathbf{B}_\rho^0, \{P_c^0\}_{c=1}^C\}$ is available **then**
 - 3: Evaluate (14), (15).
 - 4: **else if** $p_c(\Theta^0, \text{DP}_t), t = 1, \dots, m$ are available **then**
 - 5: Evaluate (15).
 - 6: **end if**
 - 7: **for** $k = 1, 2, \dots, K_{\max}$ **do**
 - 8: **M-step:** solve the concave maximization

$$\begin{aligned} \Theta^k \in \arg \max_{\Theta} \quad & \tilde{\mathcal{L}}(\Theta | \Theta^{k-1}) \\ \text{s.t.} \quad & \sum_{c=1}^C P_c = 1, P_c \geq 0, \forall c, \end{aligned} \quad (18)$$
 see (24) for efficient implementation in Gaussian case.
 - 9: **E-step:** evaluate $p_c(\Theta^k, \text{DP}_t)$ for all t using (14), and the sufficient statistics using (15).
 - 10: **end for**
 - 11: **Output:** converged parameters $\Theta^{K_{\max}}$ and conditional probabilities $p_c(\Theta^{K_{\max}}, \text{DP}_t)$ for all t .
-

exists for any $\Theta, \tilde{\Theta} \in \mathfrak{T}$. Thus,

$$\min_{k=1, \dots, K_{\max}} \sup_{\Theta \in \mathfrak{T}} \frac{\mathcal{L}'(\Theta^k; \Theta - \Theta^k)}{\|\Theta^k - \Theta\|} = \mathcal{O}\left(\sqrt{\frac{L}{K_{\max}}}\right). \quad (22)$$

Note that if $\mathcal{L}'(\bar{\Theta}; \Theta - \bar{\Theta}) \leq 0$ for all $\Theta \in \mathfrak{T}$, then $\bar{\Theta}$ is a stationary point to the MAP problem (7). As such, Algorithm 1 finds a stationary point to (7) at a sublinear rate. A key challenge in our analysis is that the MAP problem (7) is non-smooth due to the sparse/low-rank priors in (8). We achieve the proof through extending [48], [49], see Appendix A.

Implementation Details. We comment on the M-step. First, the maximizer for $\{P_c\}_{c=1}^C$ is given by:

$$P_c^* = \overline{P}_c^{\tilde{\Theta}} (\sum_{c'=1}^C \overline{P}_{c'}^{\tilde{\Theta}})^{-1}, \quad c = 1, \dots, C. \quad (23)$$

Second, the parameters $\{\mathbf{B}_\rho, \{\mathbf{L}_c\}_{c=1}^C\}$ can be obtained through solving the regularized least square problem:

$$\begin{aligned} \min_{\{\mathbf{L}_c\}_{c=1}^C, \mathbf{B}_\rho} \quad & \lambda_L \sum_{c=1}^C \|\mathbf{L}_c\|_* + \lambda_S \|\mathbf{B}_\rho\|_1 + \frac{1}{2\sigma^2} \left\{ \right. \\ & \left. \sum_{c=1}^C \sum_{i=1}^n \|e_i^\top (\mathbf{L}_c + \mathbf{B}_\rho) \overline{\mathbf{Z}}_{c,i}^{\tilde{\Theta}} - e_i^\top \overline{\mathbf{Y}\mathbf{Z}}_c^{\tilde{\Theta}} (\overline{\mathbf{Z}\mathbf{Z}}_{c,i}^{\tilde{\Theta}})^{-1}\|_F^2 \right\}, \end{aligned} \quad (24)$$

where $\overline{\mathbf{Z}}_{c,i}^{\tilde{\Theta}}$ is the matrix square root of $\overline{\mathbf{Z}\mathbf{Z}}_{c,i}^{\tilde{\Theta}}$. Note (24) is a convex robust PCA problem [47] which can be efficiently solved by available software such as [47]. Algorithm 1 also supports initialization in the absence of Θ^0 . In fact, it suffices to initialize the algorithm through evaluating the sufficient statistics in the E-step. For the latter, we estimate the conditional probability that the t th data tuple is associated to the c th graph, e.g. by applying the naïve SC. The sufficient statistics can then be found using (15).

Finally, we demonstrate how to tackle Problem 1 using the outputs from Algorithm 1. The operations are straightforward:

(i) the eigen-centrality can be estimated by applying SVD on the matrices $\{\mathbf{L}_c^{K_{\max}}\}_{c=1}^C$ and extract the top left singular vectors; (ii) the graph identifiers are estimated by taking

$$\hat{w}_t = \arg \max_{c=1, \dots, C} p_c(\Theta^{K_{\max}}, \text{DP}_t), \quad (25)$$

for all $t = 1, \dots, m$.

A. Extension to Logit Model

We conclude this section by extending Algorithm 1 to tackling Problem 1 with *binary* graph signals observations. For example, this applies if the latter consists of vote data. Consider the case without missing data, i.e., $\Omega_t = \mathbf{1}$ and focus on a logit observation model. The observed data $\{\text{DP}_t\}_{t=1}^m = \{\mathbf{y}_t, \mathbf{z}_t\}_{t=1}^m$ satisfy:

$$\mathbb{P}(y_{t,j} = Y) = \frac{\exp((\tilde{y}_{t,j} + b)Y)}{1 + \exp(\tilde{y}_{t,j} + b)}, \quad Y \in \{0, 1\}, \quad (26)$$

for $j = 1, \dots, n$, where $b < 0$ is the bias parameter of the logit model and $\tilde{y}_{t,j}$ is the j th element of the vector:

$$\tilde{\mathbf{y}}_t = \sum_{c=1}^C \mathbb{1}(w_t = c) \mathcal{H}(\mathbf{A}^{(c)}) \mathbf{B} \mathbf{z}_t. \quad (27)$$

Similar to Sec. II-A, we further adopt the parameterization with $\mathcal{H}(\mathbf{A}^{(c)}) \mathbf{B} = \mathbf{L}_c + \mathbf{B}_\rho$.

The EM algorithm on the above model can be developed similarly as Algorithm 1. In particular, the derivations up to (11) remain valid. Now, denote the conditional probability of the graph identifier w_t [cf. (14)] for the t th data tuple as:

$$p_c^{\text{lg}}(\tilde{\Theta}, \text{DP}_t) = \frac{\tilde{P}_c \prod_{j=1}^n \frac{\exp(y_{t,j} \tilde{\nu}_{t,j,c})}{1 + \exp(\tilde{\nu}_{t,j,c})}}{\sum_{c'=1}^C \tilde{P}_{c'} \prod_{j=1}^n \frac{\exp(y_{t,j} \tilde{\nu}_{t,j,c'})}{1 + \exp(\tilde{\nu}_{t,j,c'})}}, \quad (28)$$

where $\tilde{\nu}_{t,j,c} := b + \mathbf{e}_j^\top (\tilde{\mathbf{L}}_c + \tilde{\mathbf{B}}_\rho) \mathbf{z}_t$. We observe that the following surrogate objective function lower bounds the MAP objective function with the logit model (26):

$$\begin{aligned} \tilde{\mathcal{L}}_{\text{logit}}(\Theta | \tilde{\Theta}) &= \text{constant} - \lambda_S \|\mathbf{B}_\rho\|_1 - \sum_{c=1}^C \lambda_L \|\mathbf{L}_c\|_* \\ &+ \frac{1}{m} \sum_{t=1}^C \sum_{t=1}^m p_c^{\text{lg}}(\tilde{\Theta}, \text{DP}_t) \left\{ \log(P_c) + \sum_{j=1}^n y_{t,j} \nu_{t,j,c} \right\} \\ &- \frac{1}{m} \sum_{c=1}^C \sum_{t=1}^m p_c^{\text{lg}}(\tilde{\Theta}, \text{DP}_t) \sum_{j=1}^n \log(1 + \exp(\nu_{t,j,c})), \end{aligned} \quad (29)$$

where $\nu_{t,j,c} := b + \mathbf{e}_j^\top (\mathbf{L}_c + \mathbf{B}_\rho) \mathbf{z}_t$ is a linear function of the decision variables $\mathbf{L}_c, \mathbf{B}_\rho$.

We observe that (29) is a concave function in Θ . To develop the EM algorithm, the M-step in Algorithm 1 can now be replaced by maximizing (29) w.r.t. Θ when Θ^{k-1} is given. On the other hand, E-step only involves evaluating $p_c^{\text{lg}}(\tilde{\Theta}, \text{DP}_t)$ according to (28). Compared to the case with Gaussian observation, the M-step involves (29) which is a finite-sum problem that can be difficult to optimize when $m \gg 1$. This is caused by the nonlinear log-likelihood function associated with the logit model (26).

IV. ONLINE EM ALGORITHM

This section considers tackling Problem 1 under *streaming data*. We focus on an online learning process where the data tuple is revealed sequentially. Particularly, at time t , we only observe the data tuple $\text{DP}_t = \{\mathbf{y}_t, \mathbf{z}_t, \Omega_t\}$ that is generated from the model (2) in an i.i.d. fashion.

We aim to design an *online* algorithm for the MAP problem (7) with stochastic log-likelihood objective. Consider the following surrogate problem at the t th iteration:

$$\begin{aligned} &\max_{\Theta} \mathbb{E}_{\text{DP}, W \sim q(\cdot | \Theta^{t-1}, \text{DP})} [\log p(\mathbf{Y}, W | \Theta, \mathbf{Z}, \Omega)] - \Psi(\Theta) \\ &\text{with } \Psi(\Theta) := \lambda_S \|\mathbf{B}_\rho\|_1 + \lambda_L \sum_{c=1}^C \|\mathbf{L}_c\|_* \\ &\quad + \epsilon \sum_{c=1}^{C-1} \log(P_c) + \epsilon \log(1 - \sum_{c=1}^{C-1} P_c), \end{aligned} \quad (30)$$

where the expectation $\mathbb{E}_{\text{DP}}[\cdot]$ is taken w.r.t. the random generative model for the data tuple $\text{DP} = \{\mathbf{Y}, \mathbf{Z}, \Omega\}$, and $\lambda_S, \lambda_L, \epsilon > 0$ are regularization parameters. Compared to (12), the additional regularizer on $\{P_c\}_{c=1}^C$ enforces the latter to be in the interior of the simplex set.

The surrogate objective function of (30) admits a similar form as (16), which is derived as (constants are omitted)

$$\begin{aligned} \tilde{\mathcal{L}}_{\text{ol}}(\Theta; \bar{P}_c^{\Theta^{t-1}}, \bar{\mathbf{Y}} \bar{\mathbf{Z}}_c^{\Theta^{t-1}}, \bar{\mathbf{Z}} \bar{\mathbf{Z}}_{c,i}^{\Theta^{t-1}}, \forall c, i) &:= -\Psi(\Theta) \\ &+ \sum_{c=1}^C \left\{ \bar{P}_c^{\Theta^{t-1}} \log(P_c) + \frac{1}{\sigma^2} \text{Tr}((\mathbf{L}_c + \mathbf{B}_\rho)^\top \bar{\mathbf{Y}} \bar{\mathbf{Z}}_c^{\Theta^{t-1}}) \right. \\ &\left. - \frac{1}{2\sigma^2} \sum_{i=1}^n \text{Tr}((\mathbf{L}_c + \mathbf{B}_\rho)^\top \mathbf{e}_i \mathbf{e}_i^\top (\mathbf{L}_c + \mathbf{B}_\rho) \bar{\mathbf{Z}} \bar{\mathbf{Z}}_{c,i}^{\Theta^{t-1}}) \right\}, \end{aligned} \quad (31)$$

where we have defined the *population sufficient statistics* as:

$$\begin{aligned} \bar{P}_c^{\Theta^{t-1}} &= \mathbb{E}_{\text{DP}}[p_c(\Theta^{t-1}, \text{DP})], \\ \bar{\mathbf{Z}} \bar{\mathbf{Z}}_{c,i}^{\Theta^{t-1}} &= \mathbb{E}_{\text{DP}}[p_c(\Theta^{t-1}, \text{DP}) \Omega_i \mathbf{Z} \mathbf{Z}^\top], \\ \bar{\mathbf{Y}} \bar{\mathbf{Z}}_c^{\Theta^{t-1}} &= \mathbb{E}_{\text{DP}}[p_c(\Theta^{t-1}, \text{DP}) \Omega \odot \mathbf{Y} \mathbf{Z}^\top], \end{aligned} \quad (32)$$

such that $p_c(\Theta^{t-1}, \text{DP})$ was defined in (14). Note that (31), (32) generalize (15), (16) to observations drawn from any distribution. To see this, (15) can be recovered from (32) as the special case with empirical distribution.

Following the development of the batch EM algorithm, we wish to maximize (31) w.r.t. Θ at the M-step. However, unlike (15), computing (32) is challenging as we are observing the data tuple on-the-fly. To this end, we adopt the stochastic approximation (SA) scheme [50] from [51], [52] on the space of *sufficient statistics* to dynamically track (32).

SA Scheme for (32). Let $\bar{P}_c^{t-1}, \bar{\mathbf{Y}} \bar{\mathbf{Z}}_c^{t-1}, \bar{\mathbf{Z}} \bar{\mathbf{Z}}_{c,i}^{t-1}$ be the estimate for the sufficient statistics at iteration $t-1$, we consider the following SA scheme to estimate (32):

$$\begin{aligned} \bar{P}_c^t &= \bar{P}_c^{t-1} + \beta_t (p_c(\Theta^{t-1}, \text{DP}_t) - \bar{P}_c^{t-1}), \\ \bar{\mathbf{Y}} \bar{\mathbf{Z}}_c^t &= \bar{\mathbf{Y}} \bar{\mathbf{Z}}_c^{t-1} + \beta_t (p_c(\Theta^{t-1}, \text{DP}_t) \Omega_t \odot \mathbf{y}_t \mathbf{z}_t^\top - \bar{\mathbf{Y}} \bar{\mathbf{Z}}_c^{t-1}), \\ \bar{\mathbf{Z}} \bar{\mathbf{Z}}_{c,i}^t &= \bar{\mathbf{Z}} \bar{\mathbf{Z}}_{c,i}^{t-1} + \beta_t (p_c(\Theta^{t-1}, \text{DP}_t) \Omega_{t,i} \mathbf{z}_t \mathbf{z}_t^\top - \bar{\mathbf{Z}} \bar{\mathbf{Z}}_{c,i}^{t-1}), \end{aligned} \quad (33)$$

for $i = 1, \dots, n, c = 1, \dots, C$, where $\beta_t \in (0, 1]$ is the step size. Notice that the SA scheme only uses the current data DP_t available in the streaming data setting, where it replaces the E-step in the EM algorithm. The above estimates are then used in

Algorithm 2 Online EM for Partial Inference on (2)

- 1: **Input:** no. of graphs C , initial parameters Θ^0 and sufficient statistics $\{\bar{P}_c^0, \bar{Y}\bar{Z}_c^0, \{\bar{Z}\bar{Z}_{c,i}^0\}_{i=1}^n\}_{c=1}^C$.
 - 2: **for** $t = 1, 2, \dots$ **do**
 - 3: **Sample:** $\text{DP}_t = \{\mathbf{y}_t, \mathbf{z}_t, \boldsymbol{\Omega}_t\}$ according to (2).
 - 4: *// Optional: Anomaly Detection //*
 $\left\{ \begin{array}{l} \text{go to line 5, if (38) outputs } \mathcal{H}_0, \\ \text{go to line 3, if (38) outputs } \mathcal{H}_1. \end{array} \right.$
 - 5: **E-step:** update the sufficient statistics via (33).
 - 6: **M-step:** maximize the surrogate function through solving

$$\Theta^t \in \arg \max_{\Theta} \tilde{\mathcal{L}}_{\text{ol}}(\Theta; \bar{P}_c^t, \bar{Y}\bar{Z}_c^t, \bar{Z}\bar{Z}_{c,i}^t, \forall c, i).$$
 - 7: **end for**
-

(31) to construct the surrogate $\tilde{\mathcal{L}}_{\text{ol}}(\Theta; \bar{P}_c^t, \bar{Y}\bar{Z}_c^t, \bar{Z}\bar{Z}_{c,i}^t, \forall c, i)$, whose maximization leads to the M-step.

To understand (33), let us focus on \bar{P}_c^t for the illustration purpose. Herein, the *mean field* of SA update is given by the expected value of the drift term conditioned on iterates up to the $t - 1$ th iteration. The latter is

$$\mathbb{E}_{t-1}[p_c(\Theta^{t-1}, \text{DP}_t) - \bar{P}_c^{t-1}] = \mathbb{E}_{\text{DP}}[p_c(\Theta^{t-1}, \text{DP})] - \bar{P}_c^{t-1}.$$

Substituting into (32) shows that in expectation, \bar{P}_c^t is a convex combination of \bar{P}_c^{t-1} and $\bar{P}_c^{\Theta^{t-1}}$. In other words, the recursion (33) drives the sufficient statistics estimates towards (32).

Equipped with the above derivations, we summarize the online EM algorithm in Algorithm 2. Note that the algorithm is fully online as it does not store the history of $\{\text{DP}_t\}_{t \geq 0}$. Instead, information from the latter is absorbed by the sufficient statistics estimates in each iteration. Lastly, though Algorithm 2 bears similarities to [51], [52], our algorithm incorporates a set of non-smooth regularizers, i.e., $\|\mathbf{B}_\rho\|_1, \|\mathbf{L}_c\|_*$ that are motivated by the graph signal model.

Lastly, let us comment on the fixed point for the recursions (32). Note that a fixed point $(\bar{P}_c, \bar{Y}\bar{Z}_c, \bar{Z}\bar{Z}_{c,i})$ for the recursion satisfies for any $c = 1, \dots, C$ that

$$\begin{aligned} \mathbb{E}_{\text{DP}}[p_c(\bar{\Theta}, \text{DP})] - \bar{P}_c &= 0, \\ \mathbb{E}_{\text{DP}}[p_c(\bar{\Theta}, \text{DP})\boldsymbol{\Omega} \odot \mathbf{Y}\mathbf{Z}^\top] - \bar{Y}\bar{Z}_c &= 0, \\ \mathbb{E}_{\text{DP}}[p_c(\bar{\Theta}, \text{DP})\boldsymbol{\Omega}_i\mathbf{Z}\mathbf{Z}^\top] - \bar{Z}\bar{Z}_{c,i} &= 0, \quad \forall i, \end{aligned} \quad (34)$$

where $\bar{\Theta} \in \arg \max_{\Theta} \tilde{\mathcal{L}}_{\text{ol}}(\Theta; \bar{P}_c, \bar{Y}\bar{Z}_c, \bar{Z}\bar{Z}_{c,i})$. Observe:

Proposition 2 *Let Γ be the set of stationary solutions of the MAP problem with modified regularizer [cf. (7), (30)]:*

$$\max_{\Theta} \mathbb{E}_{\text{DP}}[\log p(\mathbf{Y}|\Theta, \mathbf{Z}, \boldsymbol{\Omega})] - \Psi(\Theta), \quad (35)$$

If the sufficient statistics $(\bar{P}_c, \bar{Y}\bar{Z}_c, \bar{Z}\bar{Z}_{c,i}, \forall c, i)$ satisfies (34), then $\bar{\Theta} \in \Gamma$. Conversely, assume in addition, the maximizer of $\tilde{\mathcal{L}}_{\text{ol}}(\Theta; \bar{P}_c, \bar{Y}\bar{Z}_c, \bar{Z}\bar{Z}_{c,i})$ is unique for any sufficient statistics [cf. line 6 of Algorithm 2]. Then if $\bar{\Theta} \in \Gamma$, the tuple $(\bar{P}_c, \bar{Y}\bar{Z}_c, \bar{Z}\bar{Z}_{c,i}, \forall c, i)$ satisfies (34).

The proof, which extends [51], [53] to the regularized MAP setting in (35), is relegated to Appendix B.

The above proposition shows that if the SA recursion (33) converges to a fixed point, then such fixed point must lead to the parameter $\bar{\Theta}$ stationary to the MAP problem (35). The convergence of (33) to a fixed point typically requires

$$\sum_{t=1}^{\infty} \beta_t = \infty, \quad \sum_{t=1}^{\infty} \beta_t^2 < \infty, \quad (36)$$

and additional conditions such as Lipschitz continuity of the population sufficient statistics map (32). In the interest of space, the readers are referred to [52], [54] for details. We remark that the stochastic gradient EM algorithm in [55] is an alternative to Algorithm 2. However, [55] applies stochastic gradient in the parameter (Θ) space, which can be less computationally efficient.

A. Online Joint Inference & Anomaly Detection

We conclude by discussing an application of Algorithm 2 to *online* joint inference and anomaly detection of graph signals that are not generated from one of the candidate graphs, $G^{(c)}$, $c = 1, \dots, C$, in (2). Detecting if graph signals are originated from an ‘abnormal’ graph is an important task for, e.g., power systems, pathological signal detection, see [30], [33]. While prior works require the normal graph topology to be known a-priori, our goal is to simultaneously perform graph inference through estimating central nodes and detect these abnormal graph signals. In this setting, an *online* algorithm is preferred as we aim to detect anomalies as soon as possible.

At time $t \geq 1$, we consider the graph signal \mathbf{y}_t (and the latent variable \mathbf{z}_t) satisfying $\mathbf{y}_t = \boldsymbol{\Omega}_t \odot \mathcal{H}(\mathbf{A}_t)\mathbf{B}\mathbf{z}_t + \mathbf{e}_t$ akin to (2). Herein, \mathbf{A}_t denotes the adjacency matrix of a graph G_t that \mathbf{y}_t is originated from. Accordingly, \mathbf{y}_t is said to be a *normal signal* if $G_t \in \{G^{(c)}\}_{c=1}^C$; conversely, the signal is said to be *abnormal* if it is generated from an outlier graph $G_t \notin \{G^{(c)}\}_{c=1}^C$. We define the binary hypothesis classes:

$$\begin{aligned} (\text{normal}) \quad \mathcal{H}_0 &: G_t \in \{G^{(c)}\}_{c=1}^C, \\ (\text{abnormal}) \quad \mathcal{H}_1 &: G_t \notin \{G^{(c)}\}_{c=1}^C. \end{aligned} \quad (37)$$

We shall work with cases where \mathcal{H}_1 occurs with a lower probability than \mathcal{H}_0 to allow for successful graph inference. Moreover, under \mathcal{H}_1 , the outlier graph is sufficiently different from the normal graphs in terms of its eigencentality.

Under \mathcal{H}_1 , we expect the distance $\min_{c=1, \dots, C} \|\mathbf{y}_t - \boldsymbol{\Omega}_t \odot \mathcal{H}(\mathbf{A}^{(c)})\mathbf{B}\mathbf{z}_t\|^2$ to be small under \mathcal{H}_0 and large under \mathcal{H}_1 . While determining such distance would require knowledge of the normal graphs, we utilize the online EM algorithm and replace the latter using up-to-date estimates. This leads to the online detector: let $\kappa > 0$ be a user-defined threshold,

$$\min_{c=1, \dots, C} \|\mathbf{y}_t - \boldsymbol{\Omega}_t \odot (\mathbf{L}_c^{t-1} + \mathbf{B}_\rho^{t-1})\mathbf{z}_t\|^2 \stackrel{\mathcal{H}_0}{\leq} \stackrel{\mathcal{H}_1}{\geq} \kappa. \quad (38)$$

Note that $\mathbf{L}_c^{t-1} + \mathbf{B}_\rho^{t-1} \approx \mathcal{H}(\mathbf{A}^{(c)})\mathbf{B}$ and the estimation quality improves as Algorithm 2 gathers more data samples. We expect the detection performance to improve as t grows. Finally, we incorporate the outlier rejection mechanism into Algorithm 2 by a slight modification; see line 4.

Remark 3 Compared to [30], [33], our approach requires additional information on the excitation parameter \mathbf{z}_t . On the other hand, our approach is capable of simultaneous graph learning and abnormal graph detection.

V. NUMERICAL EXPERIMENTS

In this section, we compare the performance of our EM algorithms on tackling Problem 1 for synthetic and real data with state-of-the-art algorithms.

A. Experiments on Synthetic Data

We describe the setup used throughout for synthetic data. We generate C core-periphery (CP) graphs with $n = 100$ nodes. For $c = 1, \dots, C$, the node set $\mathcal{V} = \{1, \dots, n\}$ is partitioned into a core set $\mathcal{V}_o^{(c)}$ with size $|\mathcal{V}_o^{(c)}| = 10$ and a non-core set $\mathcal{V}_p^{(c)} = \mathcal{V} \setminus \mathcal{V}_o^{(c)}$. Each node in $\mathcal{V}_o^{(c)}$ is chosen uniformly at random such that $\mathcal{V}_o^{(c)} \neq \mathcal{V}_o^{(c')}$ if $c \neq c'$. For any $i, j \in \mathcal{V}$, an edge is assigned with probability 1 if $i, j \in \mathcal{V}_o^{(c)}$; with probability 0.2 if $i \in \mathcal{V}_o^{(c)}, j \in \mathcal{V}_p^{(c)}$; and with probability 0.05 if $i, j \in \mathcal{V}_p^{(c)}$. Each observed signal \mathbf{y}_t is generated through the mixture model (2) with the noise variance of $\sigma^2 = 10^{-2}$. The graph identifier w_t is drawn uniformly from $\{1, \dots, C\}$. The missing information vector $\boldsymbol{\Omega}_t$ composes of Bernoulli r.v.s with $\mathbb{E}[\boldsymbol{\Omega}_t] = \boldsymbol{\gamma} \in [0, 1]$. For the excitation, the matrix $\mathbf{B} \in \mathbb{R}^{n \times r}$ is generated as $B_{ij} = M_{ij} \tilde{B}_{ij}$, where M_{ij}, \tilde{B}_{ij} are independent r.v.s, $M_{ij} \in \{0, 1\}$ is Bernoulli with $\mathbb{E}[M_{ij}] = 0.1$, and $\tilde{B}_{ij} \sim \mathcal{U}([0.1, 1])$. The latent parameter matrix $\mathbf{z}_t \in \mathbb{R}^r$ is generated by $[\mathbf{z}_t]_i = N_{it} \tilde{Z}_{it}$, where N_{it}, \tilde{Z}_{it} are independent r.v.s, $N_{it} \in \{0, 1\}$ is Bernoulli with $\mathbb{E}[N_{it}] = 0.6$, and $\tilde{Z}_{it} \sim \mathcal{U}([0.1, 1])$. Unless otherwise specified, the excitation rank will be set at $r = 40$.

We evaluate the performance of (A) central nodes detection and (B) graph signals clustering. For (A), we compare the mismatch between the ground truth $\mathcal{V}_o^{(c)}, c = 1, \dots, C$ and the detected central nodes via the average error rate:

$$\text{Error rate} = 1.0 - (1/C) \sum_{c=1}^C \mathbb{E} \left[\frac{1}{10} |\mathcal{V}_o^{(c)} \cap \hat{\mathcal{V}}_o^{(c)}| \right], \quad (39)$$

where $\hat{\mathcal{V}}_o^{(c)}$ is the top-10 central nodes detected in graph $G^{(c)}$ with the algorithm. For (B), we compute the normalized mutual information (NMI) [56] between the detected graph identifiers $\{\hat{w}_t\}_{t=1}^m$ and the ground truth identifiers $\{w_t\}_{t=1}^m$. A large NMI value indicates a high clustering accuracy.

Batch Algorithms. We initialize Algorithm 1 by assigning the conditional probabilities using the SC method. Let $\mathbf{U} \in \mathbb{R}^{m \times C}$ be the collection of top- C eigenvectors of data correlation matrix $\mathbf{Y}^\top \mathbf{Y}$ and $\bar{\mathbf{u}}_c$ is the centroid vector of the c th cluster computed from SC. We set:

$$p_c(\Theta^0, \text{DP}_t) = \frac{\exp(-\|\mathbf{U}_{t,:} - \bar{\mathbf{u}}_c\|^2)}{\sum_{c'=1}^C \exp(-\|\mathbf{U}_{t,:} - \bar{\mathbf{u}}_{c'}\|^2)}, \quad (40)$$

We remark that SC gives a good *initialization* to Algorithm 1 despite that the method alone may not perform well on signals originated from weak low pass filters; see Example 1.

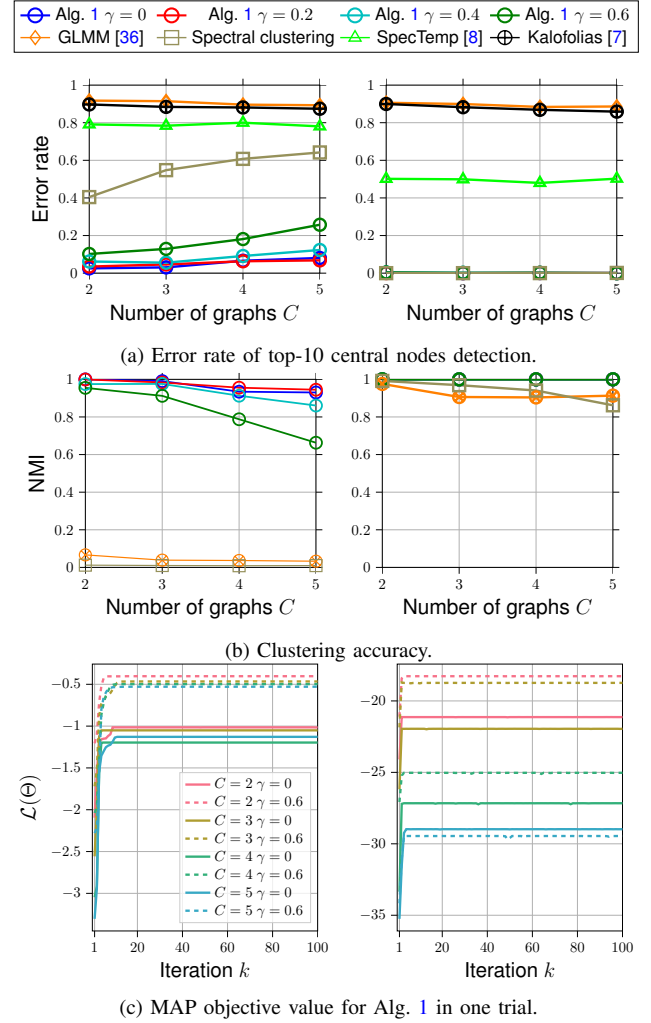


Fig. 3: Performance of the batch EM algorithm [cf. Algorithm 1] against the number of graphs C under (Left) $\mathcal{H}_w(\mathbf{A}^{(w_t)})$ and (Right) $\mathcal{H}_s(\mathbf{A}^{(w_t)})$.

The first experiment considers a batch data setting with $m = 200C$ signal tuples $\{\text{DP}_t\}_{t=1}^m$ generated from (2). The graph filters applied are $\mathcal{H}_s(\mathbf{A}^{(w_t)}) = (\mathbf{I} - \frac{1}{40} \mathbf{A}^{(w_t)})^{-1}$, $\mathcal{H}_w(\mathbf{A}^{(w_t)}) = (\mathbf{I} - \frac{1}{80} \mathbf{A}^{(w_t)})^{-1}$, where $\mathcal{H}_w(\cdot)$ is a weaker low pass filter than $\mathcal{H}_s(\cdot)$. We set $K_{\max} = 100$, $\lambda_L = 0.01$ and $\lambda_S = 0.001$. We benchmark Algorithm 1 against GLMM [36], SC, SpecTemp [8] and the method by Kalofolias [7]. To infer central nodes using the SC method, we first apply (40) to initialize the E-step and perform only one iteration of the M-step in Algorithm 1 to estimate the low rank and sparse matrices. On the other hand, a three-step procedure is simulated for [7], [8]. We first cluster data into C groups with the graph identifiers from Algorithm 1; then, we apply [7], [8] on the individual data groups to learn the corresponding graphs and compute the eigen-centrality vectors subsequently.

Fig. 3 compares the performance of algorithms against the number of graphs C with respect to the clustering accuracy (measured by NMI) and centrality detection error rate from 100 Monte-Carlo trials. First, observe that Algorithm 1 achieves significantly better performance than the benchmarks, even when a portion of observations are missing (with $\gamma > 0$). Second, under the weak low pass filter $\mathcal{H}_w(\cdot)$ (Fig. 3, Left), the

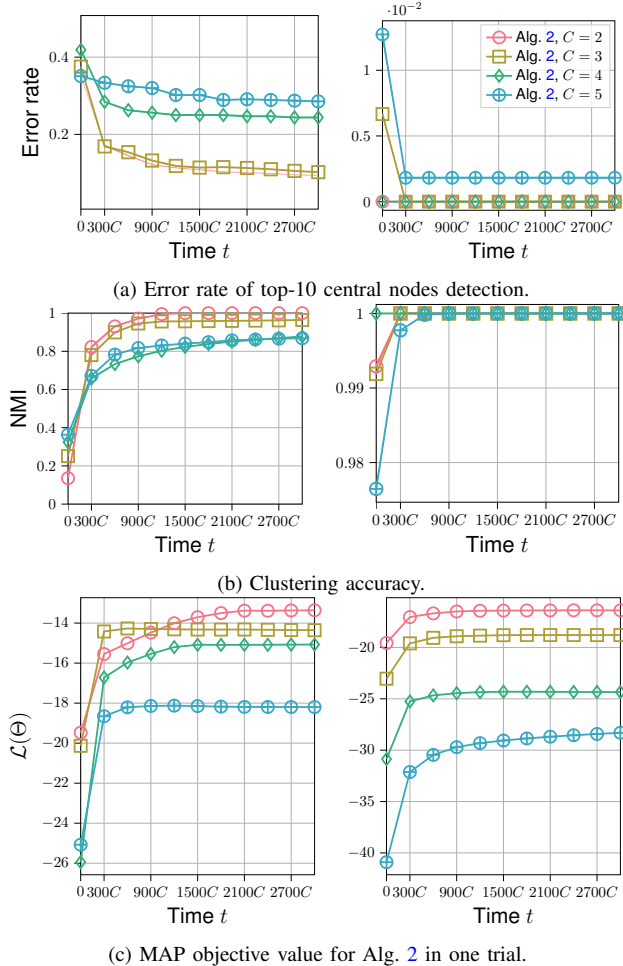


Fig. 4: Performance of the online EM algorithm [cf. Algorithm 2] against time t . (Left) $\mathcal{H}_w(\mathbf{A}^{(w_t)})$ and (Right) $\mathcal{H}_s(\mathbf{A}^{(w_t)})$.

performances of tested algorithms' worsen with the number of graphs C ; while the effect of C is less significant with the strong low pass filter $\mathcal{H}_s(\cdot)$ (Fig. 3, Right). Our results indicate that Algorithm 1 is robust to smoothness (i.e., low pass property) of graph signals and low-rank excitation.

Online Algorithm. The next experiment considers the streaming data setting where at time t , only the t th signal tuple DP_t is available and we focus on applying Algorithm 2 to continuously estimate centrality of graphs and cluster the graph signals. The data tuples are generated from (2) in the same way as in the batch data setting with no missing data, i.e., $\gamma = 0$, and we simulate the same pair of strong ($\mathcal{H}_s(\cdot)$) and weak ($\mathcal{H}_w(\cdot)$) graph filters. Note that we maintain the full dataset with $m = 3000C$ samples for benchmark. For Algorithm 2, we set $\lambda_L = 0.01$, $\lambda_S = 0.001$ and initialize the algorithm through applying Algorithm 1 on $m_{\text{init}} = 50C$ signal tuples. The step size is selected as $\beta_t = \frac{0.5}{t+m_{\text{init}}}$. We are not aware of existing works which perform simultaneous graph learning and graph signal clustering.

Fig. 4 plots the trajectories of clustering accuracy through evaluating NMI on the *full* dataset, centrality detection error rate, and the MAP objective value evaluated over the full dataset with 10 Monte-Carlo runs with the 90% confidence in-

	Alg. 1	SC	GLMM [36]	SpecTemp [8]	Kalofolias [7]
Error rate	0.15	0.73	1.00	0.71	0.91
NMI	0.93	0.18	10^{-3}	N/A	N/A

TABLE I: Tackling Problem 1 with Logit (binary) observations. The number of graphs is set as $C = 2$.

tervals. As observed, the performance of Algorithm 2 improves with time as the algorithm obtains more samples, which allows the algorithm to construct better estimate to the sufficient statistics in (33) via the SA scheme. Comparing between Fig. 4 (Left) and (Right), the terminal performance is affected by the strength of low pass graph filter as well as the model order, i.e., number of candidate graphs. The latter observation is similar to that in the batch data setting.

Logit model. Before concluding this subsection, let us also consider an application of Algorithm 1 to the logit model with batch data; cf. Sec. III-A. We consider a set of C graphs built on the simple *star graph* with $n = 20$ nodes, each with a different central node, and additional edges are assigned with probability 0.02 between the non-central nodes. In each of 30 Monte-Carlo trials, we generate $m = 80C$ data tuples according to (26). The excitation matrix \mathbf{B} follows a similar generation process as before but with $\mathbb{E}[M_{ij}] = 0.3$. The excitation rank is $r = 16$ and the tested graph filter is $\mathcal{H}(\mathbf{A}^{(w_t)}) = (\mathbf{I} - \frac{1}{30}\mathbf{A}^{(w_t)})^{-1}$. For the logit model, we set the bias parameter b as the negative average value of all signals. Lastly, Algorithm 1 is implemented in MATLAB with the CVX package [57] for solving (29). Note the benchmark algorithms are implemented through directly treating the binary observations as real-valued graph signals.

Table I compares Algorithm 1 with benchmark algorithms on tackling Problem 1 in terms of the clustering accuracy (NMI) and error rate in detecting the central node of each graph. We observe that Algorithm 1 can accurately separate the observations into C groups and detect the most central nodes inside C graphs while the benchmarks have failed in almost all 30 trials under the logit model.

B. Application: Anomaly Detection

This section considers applying Algorithm 2 to online anomaly graph detection application as described in Sec. IV-A. In the following simulation results, we consider two groups of graphs with the same size $n = 100$ and the tested graph filter is $\mathcal{H}_w(\mathbf{A}^{(w_t)})$ from Sec. V-A. The first group generates *normal graph signals* from $C = 2$ different CP graphs $\{G^{(c)}\}_{c=1}^C$. The second group generates *abnormal graph signals* via a CP graph $G^{(C+1)}$ with a different core nodes set $\mathcal{V}_o^{(C+1)}$ from $\{\mathcal{V}_o^{(c)}\}_{c=1}^C$. In our simulation, the abnormal graph signals are observed in two modes, either briefly in order or randomly. To initialize Algorithm 2, we use a set of m_{init} normal graph signals with the batch Algorithm 1.

We first compare the detector value of (38) against time t in Fig. 5. The left panel considers the case with $m_{\text{init}} = 200C$ where Algorithm 2 is initialized with a large batch of normal signals; while the right panel considers the case with

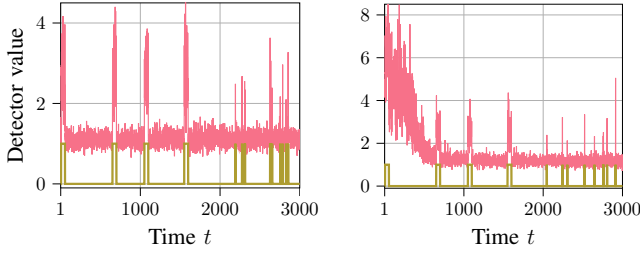


Fig. 5: Anomaly detection under $\mathcal{H}_w(\mathbf{A}^{(w_t)})$ with (Left) $m_{\text{init}} = 200C$, and (Right) $m_{\text{init}} = 20C$. Red line is the detector value of (38) against time t . Yellow line indicates when the abnormal signal is observed. If its value is 1, an abnormal signal is observed.

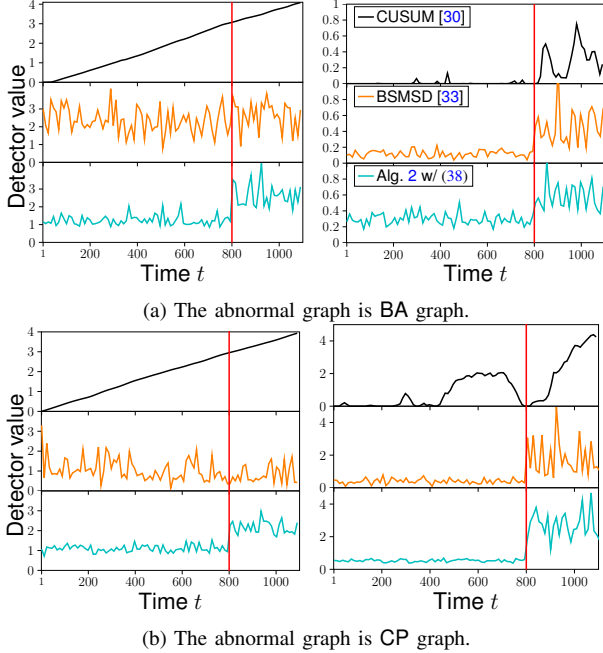


Fig. 6: Change point detection under (Left) $\mathcal{H}_w(\mathbf{A}^{(w_t)})$ and (Right) $\mathcal{H}'_{\text{bl}}(\mathbf{A}^{(w_t)})$. The detector values are normalized for better illustration. The time intervals $\{1, \dots, 400\}$, $\{401, \dots, 800\}$ refer to a 'normal region' respectively with graph $G^{(1)}$, $G^{(2)}$, and $\{801, \dots, 1100\}$ refer to a 'abnormal region' such that $t = 800$ is the change point.

$m_{\text{init}} = 20C$ where the initialization for Algorithm 2 can be inaccurate. With a large batch initialization (left panel), we observe that the detector value (38) records a significant spike over the time intervals with abnormal signals. With small batch initialization (right panel), the detector is less sensitive to the abnormal signals at the beginning. However, as time goes by and Algorithm 2 processes enough samples, (38) produces clear spikes when an abnormal graph signal is recorded.

We next study the change point detection problem which is a special case of anomaly graph detection. Our aim is to detect the time instance when the underlying graph is switched to an abnormal one. For instance, the problem is relevant for detecting events such as transmission line failure in power systems. We consider two types of abnormal graphs: CP graphs with different sets of central nodes as described previously, Barabasi–Albert (BA) graphs where each added node is connected to random $n_{\text{BA}} = 10$ existing nodes with probability proportional to their degrees. The first 800 samples are generated from normal graphs, while the remaining 300

samples are generated from abnormal graph.

We compare the detector values (38) against t with CUSUM [30], BSMSD [33]. Both existing algorithms consider the case with only one normal graph. To extend them into multiple graph settings, for the observed signal \mathbf{y}_t we compute the CUSUM/BSMSD detector values based on each normal graph $G^{(c)}$ whose topology are assumed known, then we take the minimum of the C detector values. We expect a spike in the combined detector value at the change point, i.e., the time instance when \mathbf{y}_t is generated from the abnormal graph. We consider two graph filter designs in our experiment. The first one in Fig. 6 (Left) takes the weak low pass filter $\mathcal{H}_w(\cdot)$ defined previously. The second one in Fig. 6 (Right) adopts the low pass filter defined in [33]. In the latter case, we set $\mathbf{B} = \mathbf{I}$ and the latent parameters are generated as $\mathbf{z}_t \sim \mathcal{N}(\mathbf{0}, \mathbf{I})$. The eigenvalues of the tested graph filter $\mathcal{H}'_{\text{bl}}(\cdot)$ is $\Sigma^{(w_t)}$ with $\Sigma_{ii}^{(w_t)} = \exp(-i/10)$, $i = 1, \dots, n$.

Fig. 6 presents the detector values against time t to compare the performance of three tested detectors. We observe that all detectors are able to detect the change point in the setting with graph filter $\mathcal{H}'_{\text{bl}}(\cdot)$, as seen from the pronounced spikes in detector values. Algorithm 2 has a comparable sensitivity to existing works despite the algorithm does not know the graph topology a-priori. On the other hand, under the weak low pass filter $\mathcal{H}_w(\cdot)$, Algorithm 2 still provides reliable detection on the abnormal signals. The other two detectors do not show any detectable pattern in 'normal region' and 'abnormal region'.

C. Experiments on Real Data

In this subsection, we apply the proposed algorithms on two datasets of graph signals. The first dataset (Stock) is the daily returns of S&P 100 stocks in May 2018 to Aug 2019 with $n = 99$ stocks and $m = 300$ samples, collected from <https://www.alphavantage.co/>². To estimate the excitation parameters \mathbf{Z} , we model the latter as the state of the world and consider the *interest levels* over time of $k = 5$ keywords 'trade war', 'sales tax', 'Iran', 'oil crisis', 'election' obtained from Google Trend (<https://trends.google.com>). As the stock graph may be time varying, our aim is to cluster the $m = 300$ graph signals into $C = 2$ groups and detect central stocks on the graph associated with each group of signals. We use Algorithm 1 with $\lambda_L = 1.8 \times 10^{-3}$, $\lambda_S = 1.09 \times 10^{-4}$.

For the c th clustered group of samples, denote $\mathbf{g}^{(c)}$ as the corresponding S&P100 index and $\mathbf{Y}^{(c)}$ as the individual stocks' daily returns. To measure the quality of central stocks detected, we evaluate the *normalized correlation* between the stock's daily returns and S&P100 index through

$$\text{corr}_i^{(c)} = \|\mathbf{Y}_{i,:}^{(c)}\|^{-1} \|\mathbf{g}^{(c)}\|^{-1} \langle \mathbf{Y}_{i,:}^{(c)}, \mathbf{g}^{(c)} \rangle \in [0, 1], \quad (41)$$

where $i = 1, \dots, n$. A higher correlation score indicates the corresponding stock i is a better representative of all stocks, which may imply a more central node. Fig. 7 shows the

²The Stock dataset is pre-processed by subtracting the daily returns by the minimum return value across all samples. Note that the transformed daily return values are non-negative.

	Alg. 1	SpecTemp [8]	Kalofolias [7]	GLMM [36]	SC
Max	0.81(V)	0.76(ACN)	0.76(ACN)	0.4 (MDLZ)	0.78(ACN)
Min	0.34(KO)	0.16(SO)	0.34(KO)	0.07(DUK)	0.35(MCD)
Rep.[†]	0	0.2	0.5	1	0.7

[†]Fraction of repeated central stocks detected $\frac{1}{10}|\widehat{\mathcal{V}}_o^{(1)} \cap \widehat{\mathcal{V}}_o^{(2)}|$.

TABLE II: Correlation score of top-10 detected central stocks of two graphs for Stocks dataset.

average correlation scores of top-10 detected central stocks from the corresponding groups of samples clustered by the tested algorithms. Observe that Algorithm 1 delivers higher average correlation scores than other algorithms. We also observe from Table II that Algorithm 1 detects two different groups of central stocks while other algorithms detect pairs of graphs with repeated groups of central stocks.

The second dataset (Brain) collects the functional magnetic resonance imaging (fMRI) data of 50 subjects from the Human Connectome Project with $m = 240,000$ samples, where the subjects were in resting state (RS). We use the preprocessed RS fMRI data by [28] and consider the Automated Anatomical Labeling Atlas 90 [58] for labels of brain regions. The $k = 5$ regions with largest summed absolute values of all samples are selected to form the excitation parameters \mathbf{Z} . They are left & right medial superior frontal gyrus (label 23, 24), left & right cuneus (label 45, 46) and right inferior occipital gyrus (label 54). The remaining $n = 85$ brain regions are regarded as nodes in the unknown brain graphs. To initialize Algorithm 2, we take $m_{\text{init}} = 4800$ randomly selected samples and apply the batch algorithm. We set the step size as $\beta_t = \frac{1}{t+m_{\text{init}}}$, and the MAP problem parameters are $\lambda_L = 0.45$, $\lambda_S = 0.045$.

The brain connectivity graph can vary for different resting state brain networks [28]. Fig. 8 presents the estimated centrality of $C = 3$ graphs against time while running Algorithm 2. The output of the algorithm stabilizes as more samples are observed, indicating a consistent estimation. Furthermore, the graphs $G^{(2)}$ and $G^{(3)}$ show central nodes that are concentrated in the left brain and right brain, respectively. Table III lists the labels of estimated central brain regions. For $G^{(1)}$, label 70 is Paracentral lobule [59]. It controls the movement and sensation in the lower body. For $G^{(2)}$ and $G^{(3)}$, label 12 and label 13 belong to the inferior frontal gyrus region [60], which is associated with speech and language processing.

VI. CONCLUSIONS

We study a joint graph inference problem on the challenging mixture model of filtered graph signals under general (non-white) excitation, weak low pass graph filters and missing data. We design an efficient algorithm based on EM and develop the latter's online extension for streaming data. The online algorithm is further applied to abnormal graph signals detection. Efficacy of the proposed algorithms are verified with convergence analysis and numerical experiments.

APPENDIX A

PROOF OF PROPOSITION 1

The first part follows directly from the steps of EM algorithm as the latter are majorization-minimization iterations for

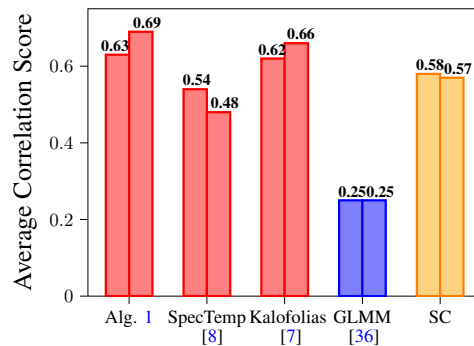


Fig. 7: Average correlation scores with the top-10 detected central stocks (in two graphs) for Stocks dataset. Red/Blue/Orange color indicates that $\mathbf{Y}^{(c)}$ are found by first clustering with Algorithm 1/GLMM [36]/SC, then the central nodes are detected with respective algorithms.

	Brain Regions with Top-10 estimated centrality value									
$G^{(1)}$	70	34	69	20	7	1	19	15	78	6
$G^{(2)}$	13	61	11	17	7	85	63	81	1	33
$G^{(3)}$	12	62	14	20	8	86	82	64	2	19

TABLE III: Labels of estimated central brain regions sorted left to right for Brain dataset.

the regularized log-likelihood. For any $k \geq 0$,

$$\mathcal{L}(\Theta^{k+1}) - \mathcal{L}(\Theta^k) \geq \tilde{\mathcal{L}}(\Theta^{k+1} | \Theta^k) - \tilde{\mathcal{L}}(\Theta^k | \Theta^k) \geq 0, \quad (42)$$

where the last inequality holds since Θ^{k+1} is a maximizer to the surrogate $\tilde{\mathcal{L}}(\Theta^{k+1} | \Theta^k)$ (16) and $\tilde{\mathcal{L}}(\Theta^k | \Theta^k) = \mathcal{L}(\Theta^k)$.

For the second part of the proposition, we observe that as $\mathcal{D}(\Theta^k | \Theta^{k-1}) = \mathcal{L}(\Theta^k) - \tilde{\mathcal{L}}(\Theta^k | \Theta^{k-1}) \leq \mathcal{L}(\Theta^k) - \mathcal{L}(\Theta^{k-1})$, where the inequality follows from $\tilde{\mathcal{L}}(\Theta^k | \Theta^{k-1}) \geq \tilde{\mathcal{L}}(\Theta^{k-1} | \Theta^{k-1}) = \mathcal{L}(\Theta^{k-1})$. Since the MAP problem has bounded objective value $\mathcal{L}(\Theta) \leq \mathcal{L}^*$. It holds

$$\sum_{k=1}^{K_{\max}} \mathcal{D}(\Theta^k | \Theta^{k-1}) \leq \mathcal{L}^* - \mathcal{L}(\Theta^0), \quad (43)$$

for any $K_{\max} \geq 1$. Now, as the gradient w.r.t. Θ of $\mathcal{D}(\Theta | \tilde{\Theta})$ is L -Lipschitz, it implies

$$\begin{aligned} 0 &\leq \mathcal{D}(\Theta^k - \frac{1}{L} \nabla \mathcal{D}(\Theta^k | \Theta^{k-1}) | \Theta^{k-1}) \\ &\leq \mathcal{D}(\Theta^k | \Theta^{k-1}) - \frac{1}{2L} \|\nabla \mathcal{D}(\Theta^k | \Theta^{k-1})\|^2, \\ &\implies \frac{1}{2L} \|\nabla \mathcal{D}(\Theta^k | \Theta^{k-1})\|^2 \leq \mathcal{D}(\Theta^k | \Theta^{k-1}). \end{aligned} \quad (44)$$

Summing up both sides from $k = 1$ to $k = K_{\max}$ and using (43) yields

$$\min_{k=1, \dots, K_{\max}} \|\nabla \mathcal{D}(\Theta^k | \Theta^{k-1})\|^2 \leq \frac{2L}{K_{\max}} (\mathcal{L}^* - \mathcal{L}(\Theta^0)). \quad (45)$$

Furthermore, the directional derivative satisfies

$$\begin{aligned} \mathcal{L}'(\Theta^k; \Theta - \Theta^k) \\ = \langle \nabla \mathcal{D}(\Theta^k | \Theta^{k-1}) | \Theta - \Theta^k \rangle + \tilde{\mathcal{L}}'(\Theta^k; \Theta - \Theta^k | \Theta^{k-1}). \end{aligned}$$

As Θ^k maximizes the concave function $\tilde{\mathcal{L}}(\Theta | \Theta^{k-1})$, it holds

$$\tilde{\mathcal{L}}'(\Theta^k; \Theta - \Theta^k | \Theta^{k-1}) \leq 0, \quad \forall \Theta \in \mathfrak{T}. \quad (46)$$

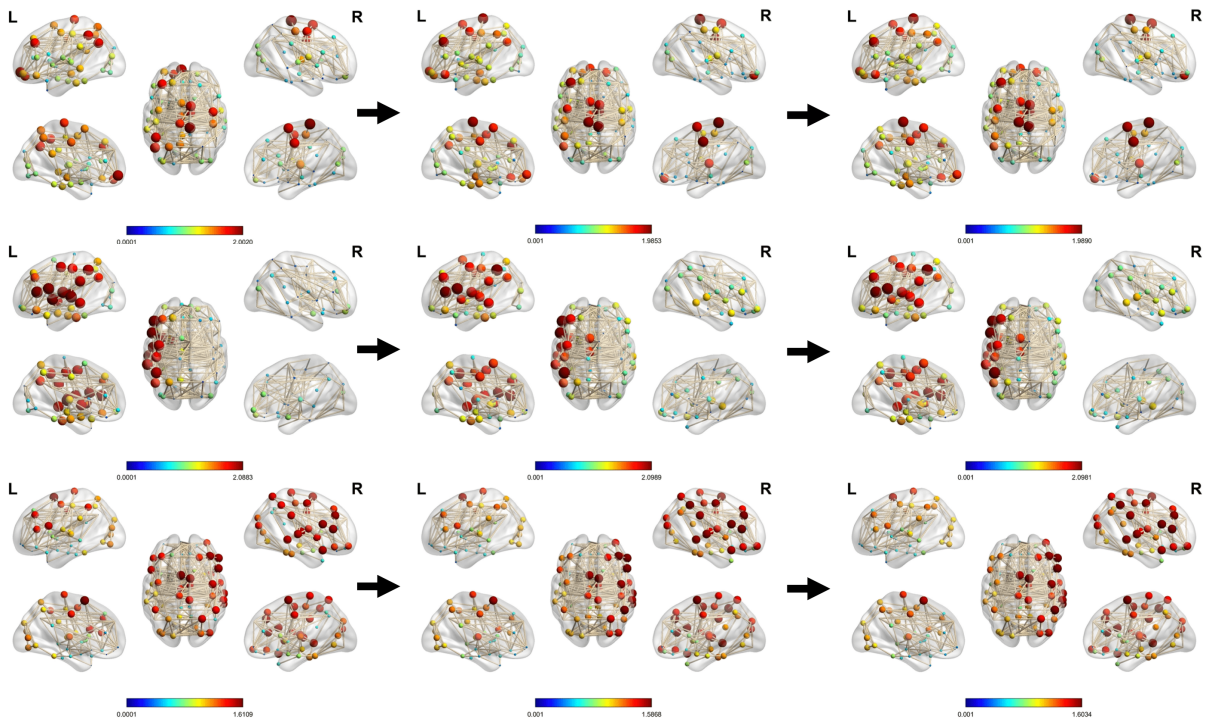


Fig. 8: Estimated centrality vectors by Algorithm 2 at time $t = 4800/134, 160/240,000$ (Left/Middle/Right). (Top) $G^{(1)}$, (Middle) $G^{(2)}$ and (Bottom) $G^{(3)}$. More central brain regions are presented with darker color and larger node size. At time $t = 240,000$, $P_1 = 0.3582$, $P_2 = 0.1562$ and $P_3 = 0.4856$.

By Cauchy-Schwarz inequality, this implies that

$$\sup_{\Theta \in \mathfrak{X}} \frac{\mathcal{L}'(\Theta^k; \Theta - \Theta^k)}{\|\Theta - \Theta^k\|} \leq \|\nabla \mathcal{D}(\Theta^k | \Theta^{k-1})\|, \quad (47)$$

where $\frac{\partial}{\partial \Theta} = 0$. Combining with (45) leads to the conclusion.

APPENDIX B PROOF OF PROPOSITION 2

To simplify notations in this proof, we denote

$$\tilde{\mathcal{L}}_{\text{ol}}(\Theta; \mathcal{S}) = \Phi(\Theta; \mathcal{S}) - \Psi(\Theta),$$

where $\mathcal{S} := (P_c, \mathbf{Y}\mathbf{Z}_c, \mathbf{Z}\mathbf{Z}_{c,i})_{c,i}$ collects the sufficient statistics, and the non-smooth function $\Psi(\Theta)$ is the regularizer and $\Phi(\Theta; \mathcal{S})$ collects the remaining terms as found in (31).

We denote $\mathcal{S}(\Theta)$ as the population sufficient statistics computed from Θ through (32). Furthermore, $\Theta(\mathcal{S}) \in \arg \max_{\Theta} \tilde{\mathcal{L}}_{\text{ol}}(\Theta; \mathcal{S})$ denotes a maximizer to the surrogate function given the sufficient statistics. Define the smooth function $f(\Theta) := \mathbb{E}_{\text{DP}}[\log p(\mathbf{Y}|\Theta, \mathbf{Z}, \Omega)]$ [cf. (35)] and

$$\Gamma = \{\Theta : 0 \in \nabla f(\Theta) - \partial \Psi(\Theta)\} \quad (48)$$

is the set of stationary points to the MAP problem (35) with the modified regularizer.

If $\bar{\mathcal{S}}$ satisfies the fixed point condition (34) where $\bar{\mathcal{S}} = \mathcal{S}(\bar{\Theta})$, we have $\bar{\Theta} \in \arg \max_{\Theta} \tilde{\mathcal{L}}_{\text{ol}}(\Theta; \bar{\mathcal{S}})$ such that

$$0 \in \partial \tilde{\mathcal{L}}_{\text{ol}}(\bar{\Theta}; \bar{\mathcal{S}}) = \nabla \Phi(\bar{\Theta}; \bar{\mathcal{S}}) - \partial \Psi(\bar{\Theta}). \quad (49)$$

By the Jensen's inequality and the fact $f(\bar{\Theta}) - \Phi(\bar{\Theta}; \bar{\mathcal{S}}) = c'$ for some constant c' , there exists $c > -\infty$ such that

$$f(\Theta) - f(\bar{\Theta}) - (\Phi(\Theta; \bar{\mathcal{S}}) - \Phi(\bar{\Theta}; \bar{\mathcal{S}})) \geq c, \quad \forall \Theta, \quad (50)$$

and the lower bound is achieved when $\Theta = \bar{\Theta}$. It implies

$$0 = \nabla f(\bar{\Theta}) - \nabla \Phi(\bar{\Theta}; \bar{\mathcal{S}}). \quad (51)$$

Inserting (51) into the fixed point condition (49) yields $\bar{\Theta} \in \Gamma$.

On the other hand, let $\bar{\Theta} \in \Gamma$ and observe the inequality (50) and its derived condition (51). Thus,

$$0 \in \nabla \Phi(\bar{\Theta}; \bar{\mathcal{S}}) - \partial \Psi(\bar{\Theta}). \quad (52)$$

As the maximizer to $\tilde{\mathcal{L}}_{\text{ol}}(\Theta; \mathcal{S})$ is unique for any \mathcal{S} , $\Theta(\bar{\mathcal{S}})$ is well defined and we conclude that $\bar{\Theta} = \Theta(\bar{\mathcal{S}})$. Furthermore, it holds that $\bar{\mathcal{S}} = \mathcal{S}(\bar{\Theta})$, which is a fixed point to (34).

REFERENCES

- [1] Y. He and H.-T. Wai, "Joint centrality estimation and graph identification from mixture of low pass graph signals," in *ICASSP*, 2022.
- [2] A. Sandryhaila and J. M. F. Moura, "Discrete signal processing on graphs," *IEEE Transactions on Signal Processing*, vol. 61, no. 7, pp. 1644–1656, 2013.
- [3] D. I. Shuman, S. K. Narang, P. Frossard, A. Ortega, and P. Vandergheynst, "The emerging field of signal processing on graphs: Extending high-dimensional data analysis to networks and other irregular domains," *IEEE Signal Processing Magazine*, vol. 30, no. 3, 2013.
- [4] A. Sandryhaila and J. M. Moura, "Big data analysis with signal processing on graphs," *IEEE Signal Processing Magazine*, vol. 31, no. 5, pp. 80–90, 2014.
- [5] Y. Tanaka, Y. C. Eldar, A. Ortega, and G. Cheung, "Sampling signals on graphs: From theory to applications," *IEEE Signal Processing Magazine*, vol. 37, no. 6, pp. 14–30, 2020.
- [6] X. Dong, D. Thanou, P. Frossard, and P. Vandergheynst, "Learning laplacian matrix in smooth graph signal representations," *IEEE Transactions on Signal Processing*, vol. 64, no. 23, pp. 6160–6173, 2016.
- [7] V. Kalofolias, "How to learn a graph from smooth signals," in *Artificial Intelligence and Statistics*, 2016, pp. 920–929.
- [8] S. Segarra, A. G. Marques, G. Mateos, and A. Ribeiro, "Network topology inference from spectral templates," *IEEE Transactions on Signal and Information Processing over Networks*, vol. 3, no. 3, 2017.

- [9] H. E. Egilmez, E. Pavez, and A. Ortega, "Graph learning from data under laplacian and structural constraints," *IEEE Journal of Selected Topics in Signal Processing*, vol. 11, no. 6, pp. 825–841, 2017.
- [10] J. Mei and J. M. Moura, "Signal processing on graphs: Causal modeling of unstructured data," *IEEE Transactions on Signal Processing*, vol. 65, no. 8, pp. 2077–2092, 2016.
- [11] Y. Shen, G. B. Giannakis, and B. Baingana, "Nonlinear structural vector autoregressive models with application to directed brain networks," *IEEE Transactions on Signal Processing*, vol. 67, no. 20, pp. 5325–5339, 2019.
- [12] H.-T. Wai, A. Scaglione, B. Barzel, and A. Leshem, "Joint network topology and dynamics recovery from perturbed stationary points," *IEEE Transactions on Signal Processing*, vol. 67, no. 17, pp. 4582–4596, 2019.
- [13] M. Coutino, E. Isufi, T. Maehara, and G. Leus, "State-space network topology identification from partial observations," *IEEE Transactions on Signal and Information Processing over Networks*, vol. 6, 2020.
- [14] X. Dong, D. Thanou, M. Rabbat, and P. Frossard, "Learning graphs from data: A signal representation perspective," *IEEE Signal Processing Magazine*, vol. 36, no. 3, pp. 44–63, 2019.
- [15] G. Mateos, S. Segarra, A. G. Marques, and A. Ribeiro, "Connecting the dots: Identifying network structure via graph signal processing," *IEEE Signal Processing Magazine*, vol. 36, no. 3, pp. 16–43, 2019.
- [16] T. M. Roddenberry and S. Segarra, "Blind inference of eigenvector centrality rankings," *IEEE Transactions on Signal Processing*, 2021.
- [17] Y. He and H.-T. Wai, "Detecting central nodes from low-rank excited graph signals via structured factor analysis," *IEEE Transactions on Signal Processing*, 2022.
- [18] H.-T. Wai, S. Segarra, A. E. Ozdaglar, A. Scaglione, and A. Jadbabaie, "Blind community detection from low-rank excitations of a graph filter," *IEEE Transactions on Signal Processing*, vol. 68, pp. 436–451, 2019.
- [19] M. T. Schaub, S. Segarra, and J. N. Tsitsiklis, "Blind identification of stochastic block models from dynamical observations," *SIAM Journal on Mathematics of Data Science*, vol. 2, no. 2, pp. 335–367, Jan 2020.
- [20] Y. Zhu, F. J. I. Garcia, A. G. Marques, and S. Segarra, "Estimating network processes via blind identification of multiple graph filters," *IEEE Transactions on Signal Processing*, vol. 68, pp. 3049–3063, 2020.
- [21] Y. He and H.-T. Wai, "Identifying first-order lowpass graph signals using perron frobenius theorem," in *ICASSP*, 2021.
- [22] D. Hallac, Y. Park, S. Boyd, and J. Leskovec, "Network inference via the time-varying graphical lasso," in *KDD*, 2017, pp. 205–213.
- [23] B. Baingana and G. B. Giannakis, "Tracking switched dynamic network topologies from information cascades," *IEEE Transactions on Signal Processing*, vol. 65, no. 4, pp. 985–997, 2016.
- [24] K. Yamada, Y. Tanaka, and A. Ortega, "Time-varying graph learning with constraints on graph temporal variation," *arXiv preprint arXiv:2001.03346*, 2020.
- [25] M. Navarro, Y. Wang, A. G. Marques, C. Uhler, and S. Segarra, "Joint inference of multiple graphs from matrix polynomials," *J. Machine Learning Research*, 2020.
- [26] X. Yang, M. Sheng, Y. Yuan, and T. Q. Quek, "Network topology inference from heterogeneous incomplete graph signals," *IEEE Transactions on Signal Processing*, vol. 69, pp. 314–327, 2020.
- [27] S. Rey, A. Buciuiea, M. Navarro, S. Segarra, and A. G. Marques, "Joint inference of multiple graphs with hidden variables from stationary graph signals," in *ICASSP*, 2022, pp. 5817–5821.
- [28] I. Ricchi, A. Tarun, H. P. Maretic, P. Frossard, and D. Van De Ville, "Dynamics of functional network organization through graph mixture learning," *NeuroImage*, vol. 252, p. 119037, 2022.
- [29] R. H. Heiberger, "Stock network stability in times of crisis," *Physica A: Statistical Mechanics and its Applications*, vol. 393, pp. 376–381, 2014.
- [30] C. Kaushik, T. M. Roddenberry, and S. Segarra, "Network topology change-point detection from graph signals with prior spectral signatures," in *ICASSP*, 2021, pp. 5395–5399.
- [31] S. P. Chepuri and G. Leus, "Subgraph detection using graph signals," in *Asilomar*, 2016, pp. 532–534.
- [32] S. Shaked and T. Routtenberg, "Identification of edge disconnections in networks based on graph filter outputs," *arXiv preprint arXiv:2102.06428*, 2021.
- [33] E. Isufi, A. S. Mahabir, and G. Leus, "Blind graph topology change detection," *IEEE Signal Processing Letters*, vol. 25, no. 5, 2018.
- [34] U. Von Luxburg, "A tutorial on spectral clustering," *Statistics and computing*, vol. 17, no. 4, pp. 395–416, 2007.
- [35] G. Guo, H. Wang, D. Bell, Y. Bi, and K. Greer, "Knn model-based approach in classification," in *ODBASE*. Springer, 2003, pp. 986–996.
- [36] H. P. Maretic and P. Frossard, "Graph laplacian mixture model," *IEEE Transactions on Signal and Information Processing over Networks*, vol. 6, pp. 261–270, 2020.
- [37] Y. Yuan, X. Yang, K. Guo, T. Q. Quek *et al.*, "Gragec: Graph signal clustering and multiple graph estimation," *IEEE Transactions on Signal Processing*, vol. 70, pp. 2015–2030, 2022.
- [38] A. Karaaslanli and S. Aviyente, "Simultaneous graph signal clustering and graph learning," in *International Conference on Machine Learning*. PMLR, 2022, pp. 10762–10772.
- [39] H. Araghi, M. Sabbaqi, and M. Babaie-Zadeh, "k-graphs: An algorithm for graph signal clustering and multiple graph learning," *IEEE Signal Processing Letters*, vol. 26, no. 10, pp. 1486–1490, 2019.
- [40] S. Vlaski, H. P. Maretic, R. Nassif, P. Frossard, and A. H. Sayed, "Online graph learning from sequential data," in *2018 IEEE Data Science Workshop (DSW)*. IEEE, 2018, pp. 190–194.
- [41] R. Shafipour and G. Mateos, "Online topology inference from streaming stationary graph signals with partial connectivity information," *Algorithms*, vol. 13, no. 9, p. 228, 2020.
- [42] V. Shumovskaia, K. Ntemos, S. Vlaski, and A. H. Sayed, "Online graph learning from social interactions," in *2021 55th Asilomar Conference on Signals, Systems, and Computers*. IEEE, 2021, pp. 1263–1267.
- [43] S. S. Saboksayr, G. Mateos, and M. Cetin, "Online discriminative graph learning from multi-class smooth signals," *Signal Processing*, vol. 186, p. 108101, 2021.
- [44] M. Udell and A. Townsend, "Why are big data matrices approximately low rank?" *SIAM Journal on Mathematics of Data Science*, vol. 1, no. 1, pp. 144–160, 2019.
- [45] M. Cucuringu, P. Rombach, S. H. Lee, and M. A. Porter, "Detection of core-periphery structure in networks using spectral methods and geodesic paths," *European Journal of Applied Mathematics*, vol. 27, no. 6, pp. 846–887, 2016.
- [46] R. Ramakrishna, H.-T. Wai, and A. Scaglione, "A user guide to low-pass graph signal processing and its applications," *IEEE Signal Processing Magazine*, 2020.
- [47] A. Agarwal, S. Negahban, M. J. Wainwright *et al.*, "Noisy matrix decomposition via convex relaxation: Optimal rates in high dimensions," *The Annals of Statistics*, vol. 40, no. 2, pp. 1171–1197, 2012.
- [48] J. Mairal, "Incremental majorization-minimization optimization with application to large-scale machine learning," *SIAM Journal on Optimization*, vol. 25, no. 2, pp. 829–855, 2015.
- [49] B. Karimi, H.-T. Wai, E. Moulines, and P. Li, "Minimization by incremental stochastic surrogate optimization for large scale nonconvex problems," in *ALT*, vol. 167, 2022, pp. 606–637.
- [50] H. Robbins and S. Monro, "A stochastic approximation method," *The annals of mathematical statistics*, pp. 400–407, 1951.
- [51] O. Cappé and E. Moulines, "On-line expectation-maximization algorithm for latent data models," *Journal of the Royal Statistical Society: Series B (Statistical Methodology)*, vol. 71, no. 3, pp. 593–613, 2009.
- [52] B. Karimi, B. Miasojedow, E. Moulines, and H.-T. Wai, "Non-asymptotic analysis of biased stochastic approximation scheme," in *Conference on Learning Theory*. PMLR, 2019, pp. 1944–1974.
- [53] H. Nguyen, F. Forbes, G. Fort, and O. Cappé, "An online minorization-maximization algorithm," 2022.
- [54] H. Kushner and G. G. Yin, *Stochastic approximation and recursive algorithms and applications*. Springer Science, 2003.
- [55] S. Balakrishnan, M. J. Wainwright, and B. Yu, "Statistical guarantees for the em algorithm: From population to sample-based analysis," *The Annals of Statistics*, vol. 45, no. 1, pp. 77–120, 2017.
- [56] N. X. Vinh, J. Epps, and J. Bailey, "Information theoretic measures for clusterings comparison: Variants, properties, normalization and correction for chance," *The Journal of Machine Learning Research*, vol. 11, pp. 2837–2854, 2010.
- [57] M. Grant and S. Boyd, "CVX: Matlab software for disciplined convex programming, version 2.1," <http://cvxr.com/cvx>, Mar. 2014.
- [58] N. Tzourio-Mazoyer, B. Landeau, D. Papathanassiou, F. Crivello, O. Etard, N. Delcroix, B. Mazoyer, and M. Joliot, "Automated anatomical labeling of activations in spm using a macroscopic anatomical parcellation of the mni mri single-subject brain," *Neuroimage*, vol. 15, no. 1, pp. 273–289, 2002.
- [59] J. C. Grotta, G. W. Albers, J. P. Broderick, S. E. Kasner, E. H. Lo, R. L. Sacco, L. K. Wong, and A. L. Day, *Stroke e-book: Pathophysiology, diagnosis, and management*. Elsevier Health Sciences, 2021.
- [60] J. D. Greenlee, H. Oya, H. Kawasaki, I. O. Volkov, M. A. Severson III, M. A. Howard III, and J. F. Brugge, "Functional connections within the human inferior frontal gyrus," *Journal of Comparative Neurology*, vol. 503, no. 4, pp. 550–559, 2007.